

Plasmas Computed with ATMED CR of the 4th Non Local Thermodynamic Equilibrium Code Comparison Workshop Database

A.J. Benita ^{a,b*}

^aPlasma Atomic Physics Group, Madrid Polytechnic University, 28006 Madrid, Spain

^bPhysics Department, Las Palmas Canary Islands University, 35017 Las Palmas de Gran Canaria, Spain

In this paper, there are presented some results calculated with code ATMED CR (**ATom MEDium Collisional Radiative**) of the 4th Non-LTE Code Comparison Workshop held in December 2005, when this software didn't exist, having been released in 2017. NLTE population kinetics codes were tested of steady-state cases for C, Ar, Fe, Sn, Xe and Au plasmas selected for detailed comparisons. Apart from analyzing dense plasma physics, the scope was expanded including the EUV lithography sources and photoionized plasmas.

The purpose of the paper is to present good results computed of ATMED CR of plasmas proposed in this scientific meeting of 2005. The results for plasma properties can be considered as relatively precise and optimal, being checked fundamentally the high sensitivity of calculations to changes in regions of local thermodynamic equilibrium (LTE) or non local thermodynamic equilibrium (NLTE), electronic and radiation temperatures, electronic density and plasma length. Frequency resolved and mean opacities are also displayed computed with ATMED CR using UTA (Unresolved Transition Array) formalism.

Keywords:

Screened Hydrogenic Atomic Model; Collisional Radiative Average Atom Code; Plasmas of NLTE-4 Workshop

*Corresponding author as partner of: Atomic Physics Group (UPM & ULPGC), Madrid, Spain.

E-mail address (A.J. Benita): anajosefa.benita@upm.es / anajosefa.benita.cerdan@alumnos.upm.es

1. INTRODUCTION

The collisional radiative model ATMED CR [1,2] constructed in the Average Atom formalism has been developed to calculate plasma population kinetics under coronal, local or non-local thermodynamic equilibrium regions as an extension of the module named ATMED LTE [3-5] designed previously for local thermodynamic conditions. The atomic model is based on a New Relativistic Screened Hydrogenic Model (NRSHM) with a set of universal screening constants including nlj -splitting that has been obtained by fitting to a large database of 61,350 atomic high quality data entries, compiled from the National Institute of Standards and Technology (NIST) database of U.S. Department of Commerce and from the Flexible Atomic Code (FAC) [6,7].

The calculation of accurate relativistic atomic populations including nlj -splitting of electronic orbitals, improves the precision of atomic properties as mean charge, rates and the resolution of spectral properties as opacities and radiative power losses, with respect to collisional radiative average atom codes as XSN of W. Lokke and W. Grasberger of 1977 with n -splitting [8,9] or considering nl -splitting [10-13]. The CR balance is based on iterative loops for reaching auto convergence in populations and plasma mean charge [14]. The accuracy ATMED CR code can achieve can be consulted in Section 3 of Ref. [15] which explains in detail the phases of the investigation project, consisting of the comparison of plasma properties of this software with bibliographic data.

The implementation of the collisional radiative balance with the new atomic model, allows now to compute plasmas in NLTE or coronal regions, widening considerably for all chemical elements the validity range of thermodynamic conditions [16,17]. In Section 2 there are modeled plasmas with ATMED CR illustrating the high agreement with results for plasma properties of other codes. Section 3 contains main conclusions. Details about the workshop, motivations for the chosen cases and discussion of some representative results can be found in References [18-20].

2. PLASMAS OF 4TH NLTE DATABASE

The problems proposed for the steady-state cases of C, Ar, Sn, Xe and Au atoms have been calculated with the collisional radiative average atom code ATMED CR. Some graphs are displayed by courtesy of the database (<https://nlte.nist.gov/NLTE4/>) for visual comparison of plasma properties.

2.1 Carbon Plasmas

The following problems have been established for the steady-state cases of carbon atoms on a grid of electron temperatures and electron densities, see Table 1 and Figure 1:

Element	Case ID	Total # of Points	Parameter	Grid	# of Points
Detailed NLTE case (proposed at NLTE-3); comparison with the benchmark theoretical results					
Carbon	C	16	T _e	3, 5, 7, 10	4
			N _e	10 ¹³ , 10 ¹⁵ , 10 ¹⁷ , 10 ¹⁹	4

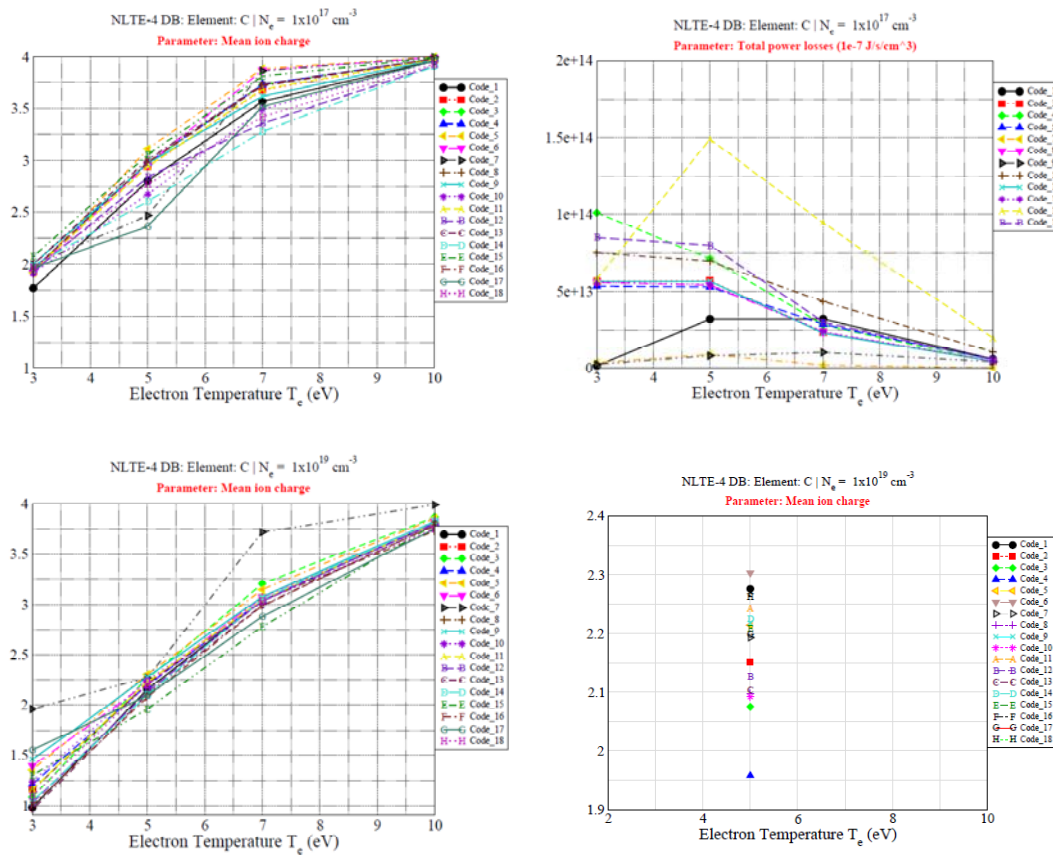


Figure 1.a. Carbon plasma properties computed with participant codes of NLTE-4 Workshop

In Figure 1 and Table 1 there are displayed values of carbon plasmas, checking the high agreement of ATMED CR results with respect to other participant codes, being as well as a snapshot of the high sensitivity to slight changes in temperatures or densities. In tables there are indicated the approximated ranges of mean charge for all plasma cases.

Table 1.a: Carbon plasma properties of ATMED CR for comparison with codes of NLTE-4 Workshop

$N_e (\text{cm}^{-3}) = 10^{13}$	ρ (g/cm ³)	Z_{bar}	Z_{bar}	η_e	K_R (cm ² /g)	K_p (cm ² /g)	RPL (1e-7 J/cm ³ /s)
$T_e = 3 \text{ eV}$	1.040E-10	1.926E+00	1.2÷2	-2.1862E+01	1.557E+01	2.638E+04	3.938131E+03
$T_e = 10 \text{ eV}$	1.015E-10	1.981E+00	3.2÷4	-2.3664E+01	1.157E+02	3.219E+05	2.521072E+05
$N_e (\text{cm}^{-3}) = 10^{15}$	ρ (g/cm ³)	Z_{bar}	Z_{bar}	η_e	K_R (cm ² /g)	K_p (cm ² /g)	RPL (1e-7 J/cm ³ /s)
$T_e = 3 \text{ eV}$	1.450E-08	1.953E+00	1.4÷2	-1.6911E+01	6.540E+01	2.485E+04	4.820444E+07
$T_e = 5 \text{ eV}$	1.500E-08	1.958E+00	1.8÷2.9	-1.7641E+01	2.830E+02	2.008E+05	4.504697E+08
$T_e = 7 \text{ eV}$	9.000E-09	2.247E+00	2.2÷3.7	-1.8518E+01	9.876E+02	2.561E+05	7.903052E+08
$T_e = 10 \text{ eV}$	5.150E-09	3.897E+00	3.3÷4	-1.9061E+01	3.811E+01	4.609E+03	2.035248E+09
$N_e (\text{cm}^{-3}) = 10^{17}$	ρ (g/cm ³)	Z_{bar}	Z_{bar}	η_e	K_R (cm ² /g)	K_p (cm ² /g)	RPL (1e-7 J/cm ³ /s)
$T_e = 5 \text{ eV}$	6.200E-07	3.222E+00	2.4÷3.2	-1.3421E+01	3.684E+04	7.617E+04	2.160765E+12
$T_e = 7 \text{ eV}$	6.000E-07	3.445E+00	3.3÷3.9	-1.3892E+01	2.530E+04	3.836E+04	3.487695E+12
$T_e = 10 \text{ eV}$	5.300E-07	3.830E+00	3.8÷4	-1.4445E+01	7.957E+02	1.192E+04	1.628114E+12
$N_e (\text{cm}^{-3}) = 10^{19}$	ρ (g/cm ³)	Z_{bar}	Z_{bar}	η_e	K_R (cm ² /g)	K_p (cm ² /g)	RPL (1e-7 J/cm ³ /s)
$T_e = 5 \text{ eV}$	9.000E-05	2.330E+00	2÷2.3	-8.7669E+00	4.637E+04	2.032E+05	2.427511E+13
$T_e = 7 \text{ eV}$	6.100E-05	3.278E+00	2.8÷3.2	-9.3195E+00	4.005E+04	5.318E+04	1.181351E+13
$T_e = 10 \text{ eV}$	5.300E-05	3.853E+00	3.7÷4	-9.8334E+00	2.367E+03	1.138E+04	6.402962E+12

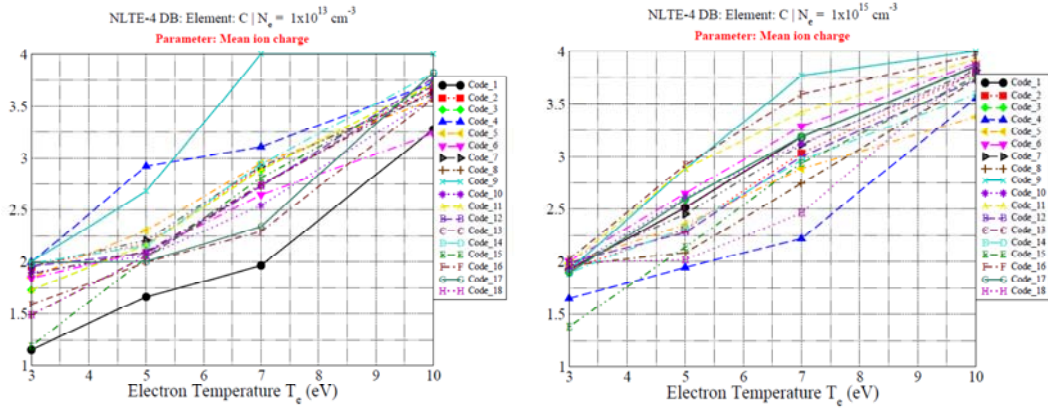


Figure 1.b. Carbon plasma properties computed with participant codes of NLTE-4 Workshop

2.2 Argon Plasmas

The following problems have been established for the steady-state cases of argon atoms on a grid of electron temperatures and electron densities, see Table 2 and Figure 2:

Element	Case ID	Total # of Points	Parameter	Grid	# of Points
The same case (almost) as in NLTE-3; non-Maxwellian; test the progress since NLTE-3					
Argon	Ar	24	T _e	50, 100, 300, 600	4
			N _e	10 ¹² , 10 ¹⁸ , 10 ²³	3
			T ₂	10 ⁴ (10 keV)	
			% of T ₂ in N _e	0 and 10%	2

Some collisional processes induced by a fraction of 10% very energetic and hot electrons have been also considered at a temperature of T_{hot} = 10 keV. Other fractions of hot electrons have been tested with ATMED CR, observing a softer influence on parameters as mean charge than with the codes of Workshop NLTE-4, supposing an additive contribution of atomic processes. The collisional ionization rate from i energy level is calculated as follows:

$$I_C^{ic} = 4\pi a_0^2 Ryd^2 \zeta_{Lotz} c \left(\frac{8}{\pi m_e c^2} \right)^{1/2} \frac{N_e^{hot}}{(K_B T_e^{hot})^{3/2}} \frac{E_1(\beta_e^{hot} I_i)}{\beta_e^{hot} I_i} \quad (s^{-1}) \quad (1)$$

- $a_0 = 0.5291772083 \times 10^{-8}$ cm : Bohr radius.
- $Ryd = -13.605698$ eV : Hydrogen atom ionization potential.
- $\zeta_{Lotz} = 0.691$: Lotz approximation parameter.
- $c = 299792458 \times 10^2$ cm/s : Speed of light.
- $m_e c^2 = 0.510998902 \times 10^6$ eV : Electron mass at rest.
- $N_e^{hot} = 0.1 * N_e$: Electronic density of hot electrons as a fraction of total density N_e .
- T_e^{hot} eV : Electronic temperature of hot electrons (10000 eV in these plasma cases) and $\beta_e^{hot} = 1/K_B T_e^{hot}$ inverse of hot electrons temperature.
- $E_1(u) = \int_1^\infty dx \frac{e^{-ux}}{x}$: First exponential integral.
- $I_i = -\epsilon_i$ eV : Ionization potential of energy level i.

The formula can be rewritten in an adequate form to implement it inside FORTRAN code as:

$$I_C^{ic} = 4.36 \times 10^{-6} \zeta_{Lotz} \frac{N_e^{hot}}{(K_B T_e^{hot})^{1/2} I_i} E_1(\beta_e^{hot} I_i) \quad (s^{-1}) \quad (2)$$

The rate of three body recombination to the energy level i, is calculated assuming LTE through detailed balance with collisional ionization:

$$R_C^{ci} = I_C^{ic} \exp[-\beta_e^{hot}(\epsilon_i - \mu_e)] \quad (s^{-1}) \quad (3)$$

Although the relation has been deduced from the hypothesis of equilibrium, this only depends on atomic magnitudes and on the temperature. For that reason, the equation will be valid in every situation always and when the free electron distribution is a Maxwellian function. The collisional excitation rate from i energy level to j one is calculated as follows:

$$\tau_{ij}^C = 16 Ryd^2 a_0^2 c \left(\frac{2\pi^3}{3m_e c^2} \right)^{1/2} \frac{f_{ij}}{D_j^0} \frac{N_e^{hot}}{(K_B T_e^{hot})^{3/2}} \frac{\exp(-\beta_e^{hot} \epsilon_{ij})}{\beta_e^{hot} \epsilon_{ij}} G(\beta_e^{hot} \epsilon_{ij}) \quad (s^{-1}) \quad (4)$$

- $\epsilon_{ij} = \epsilon_j - \epsilon_i \text{ eV}$: Excitation energy.
- f_{ij} : Bound-bound absorption oscillator strength from i energy level to j one.
- $G(u) = A + (Bu - Cu^2 + D)e^u E_1(u) + Cu$: Gaunt factor.
 - $\begin{cases} A = 0.15 & \text{si } n_j \neq n_i \\ A = 0.60 & \text{si } n_j = n_i \end{cases}$: Parameter A.
 - $B = C = 0$: Parameters B and C.
 - $D = 0.28$: Parameter D.

The formula can be rewritten in an adequate form to implement it inside FORTRAN code as:

$$\tau_{ij}^C = 1.58 \times 10^{-5} \frac{f_{ij}}{\epsilon_{ij} (K_B T_e^{hot})^{1/2}} \frac{N_e^{hot}}{D_j^0} [A \exp(-\beta_e^{hot} \epsilon_{ij}) + 0.28 E_1(\beta_e^{hot} \epsilon_{ij})] \quad (s^{-1}) \quad (5)$$

The rate of collisional de-excitation from level j to level i, is calculated assuming LTE through detailed balance with collisional excitation:

$$\tau_{ji}^C = \tau_{ij}^C \exp[\beta_e^{hot}(\epsilon_j - \epsilon_i)] \quad (s^{-1}) \quad (6)$$

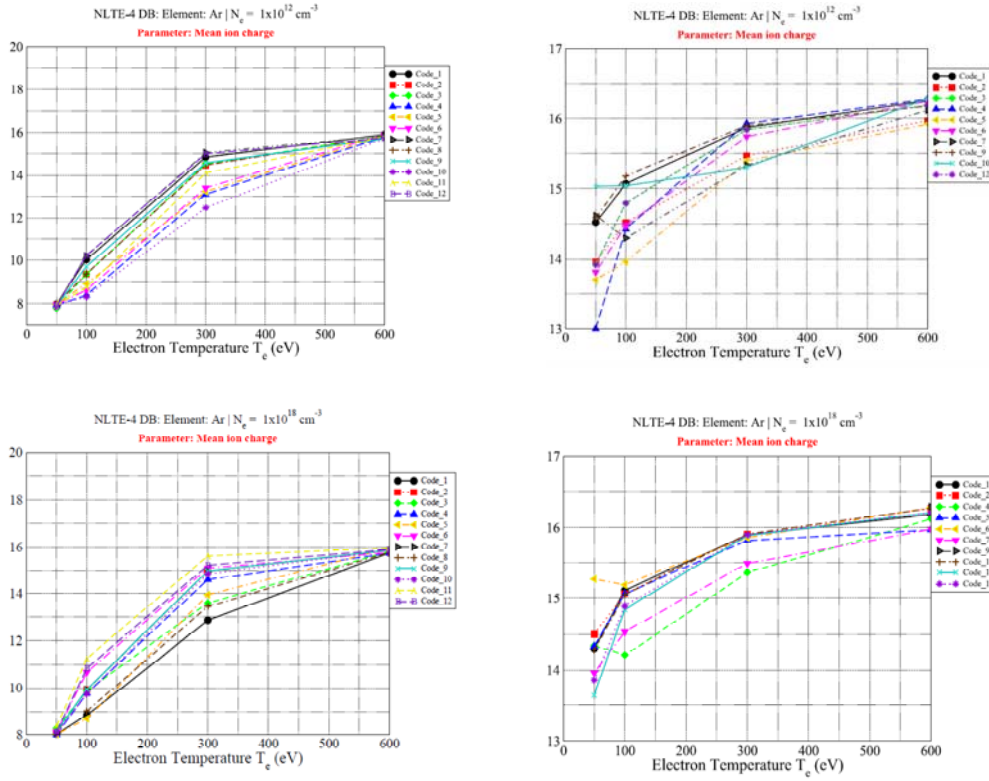


Figure 2.a: Argon plasma properties with participant codes of NLTE-4 Workshop, without (left) or with (right) hot electrons

Table 2.a: Argon plasma properties without hot electrons of ATMED CR for comparison with codes of NLTE-4 Workshop

0% Hot e- & $N_e \text{ (cm}^{-3}\text{)} = 10^{12}$	ρ (g/cm ³)	$Z_{\bar{m}}$ ATMED	$Z_{\bar{m}}$ NLTE-4	η_e ATMED CR	K_R (cm ² /g)	K_p (cm ² /g)	RPL (1e-7 J/cm ³ /s)
$T_e = 100 \text{ eV}$	8.300E-12	7.999E+00	7.5÷11	-2.9428E+01	1.174E+01	1.420E+04	2.422328E+04
$T_e = 300 \text{ eV}$	8.300E-12	8.017E+00	12÷15	-3.1074E+01	1.024E+02	4.465E+03	1.170868E+05
0% Hot e- & $N_e \text{ (cm}^{-3}\text{)} = 10^{18}$	ρ (g/cm ³)	$Z_{\bar{m}}$ ATMED	$Z_{\bar{m}}$ NLTE-4	η_e ATMED CR	K_R (cm ² /g)	K_p (cm ² /g)	RPL (1e-7 J/cm ³ /s)
$T_e = 50 \text{ eV}$	8.300E-06	8.001E+00	8÷9	-1.4573E+01	1.175E+02	8.527E+03	5.394289E+14
$T_e = 100 \text{ eV}$	8.900E-06	9.616E+00	9÷11	-1.5359E+01	1.495E+02	9.906E+03	2.107586E+15
$T_e = 300 \text{ eV}$	5.700E-06	1.183E+01	11÷15	-1.7245E+01	2.988E+02	2.507E+03	8.107686E+15
$T_e = 600 \text{ eV}$	5.500E-06	1.294E+01	15÷16	-1.8231E+01	2.281E+02	8.831E+02	1.977565E+16
0% Hot e- & $N_e \text{ (cm}^{-3}\text{)} = 10^{23}$	ρ (g/cm ³)	$Z_{\bar{m}}$ ATMED	$Z_{\bar{m}}$ NLTE-4	η_e ATMED CR	K_R (cm ² /g)	K_p (cm ² /g)	RPL (1e-7 J/cm ³ /s)
$T_e = 100 \text{ eV}$	1.130E+00	5.907E+00	8÷10	-4.0884E+00	6.302E+03	1.133E+04	2.566309E+27
$T_e = 300 \text{ eV}$	4.600E-01	1.458E+01	14÷16	-5.7365E+00	7.302E+01	5.008E+02	8.305196E+25
$T_e = 600 \text{ eV}$	4.250E-01	1.577E+01	15÷16	-6.7773E+00	6.215E+00	3.186E+02	3.273017E+25

Table 2.b: Argon plasma properties of ATMED CR for other test cases with 50% of hot electrons

50% Hot e- & $N_e \text{ (cm}^{-3}\text{)}$	ρ (g/cm ³)	$Z_{\bar{m}}$ ATMED	η_e ATMED CR	K_R (cm ² /g)	K_p (cm ² /g)	N_e (cm ⁻³)
$T_e = 100 \text{ eV}$	7.000E-06	1.022E+01	-1.5538E+01	1.215E+02	8.676E+03	1.0E+18
$T_e = 100 \text{ eV}$	8.200E-01	8.161E+00	-4.0858E+00	4.475E+03	8.810E+03	1.0E+23
$T_e = 300 \text{ eV}$	4.400E-01	1.530E+01	-5.7325E+00	3.153E+01	2.515E+02	1.0E+23

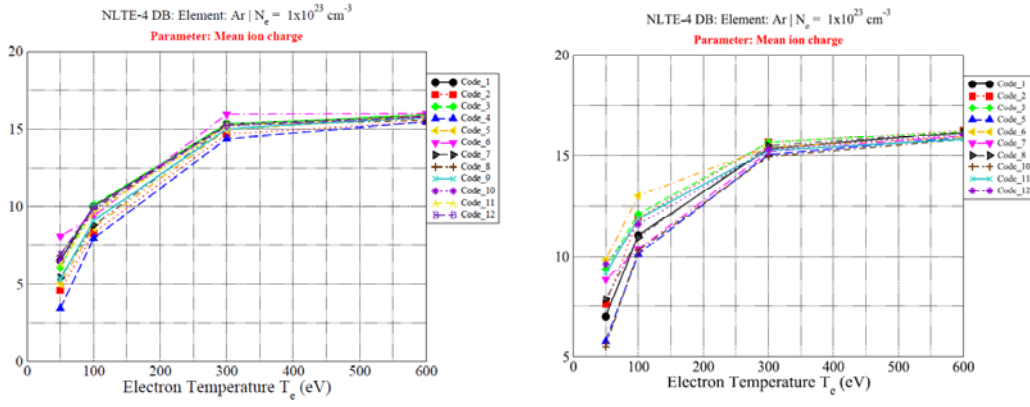


Figure 2.b. Argon plasma properties with participant codes of NLTE-4 Workshop, without (left) or with (right) hot electrons

Table 2.c: Argon plasma properties with hot electrons of ATMED CR for comparison with codes of NLTE-4 Workshop

10% Hot e- & N _e (cm ⁻³) = 10 ¹²	ρ (g/cm ³)	Z _{bar} ATMED	Z _{bar} NLTE-4	η _e ATMED CR	K _R (cm ² /g)	K _P (cm ² /g)
T _e = 50 eV	9.000E-12	8.019E+00	13÷15	-2.8305E+01	1.624E+00	8.456E+03
T _e = 100 eV	8.500E-12	8.004E+00	14÷15	-2.9404E+01	1.006E+01	1.418E+04
T _e = 300 eV	8.300E-12	8.019E+00	15÷16	-3.1074E+01	1.012E+02	4.465E+03
10% Hot e- & N _e (cm ⁻³) = 10 ¹⁸	ρ (g/cm ³)	Z _{bar} ATMED	Z _{bar} NLTE-4	η _e ATMED CR	K _R (cm ² /g)	K _P (cm ² /g)
T _e = 50 eV	8.200E-06	8.207E+00	13.5÷15	-1.4559E+01	6.618E+01	8.133E+03
T _e = 100 eV	7.000E-06	9.624E+00	14÷15	-1.5598E+01	1.420E+02	9.889E+03
T _e = 300 eV	5.700E-06	1.189E+01	15÷16	-1.7240E+01	2.960E+02	2.470E+03
T _e = 600 eV	5.500E-06	1.298E+01	16÷17	-1.8228E+01	2.269E+02	8.780E+02
10% Hot e- & N _e (cm ⁻³) = 10 ²³	ρ (g/cm ³)	Z _{bar} ATMED	Z _{bar} NLTE-4	η _e ATMED CR	K _R (cm ² /g)	K _P (cm ² /g)
T _e = 100 eV	1.700E+00	4.020E+00	10÷13	-4.0647E+00	7.890E+03	1.317E+04
T _e = 300 eV	4.600E-01	1.449E+01	15	-5.7423E+00	7.662E+01	5.223E+02
T _e = 600 eV	4.250E-01	1.573E+01	15÷16	-6.7799E+00	7.823E+00	3.151E+02

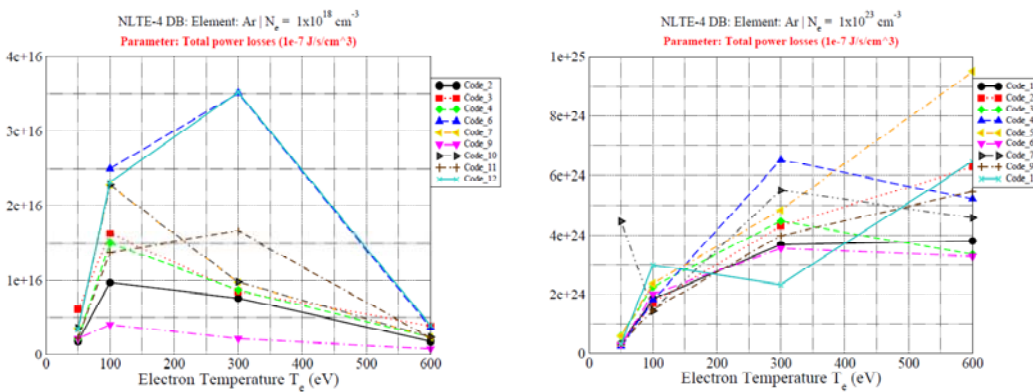


Figure 2.c. Argon plasma RPL with participant codes of NLTE-4 Workshop, without hot electrons

2.3 Tin Plasmas

The following problems have been established for the steady-state tin atoms, see Table 3, Figure 3:

Element	Case ID	Total # of Points	Parameter	Grid	# of Points
EUV lithography; includes optically thick case; spectrum emission; exp. data available					
Tin	Sn	50	T_e	20, 25, 30, 35, 40	5
			N_e	$10^{18}, 5 \times 10^{18}, 10^{19}, 5 \times 10^{19}, 10^{21}$	5
			Opacity	$r = 0$ and 0.1 mm; $L = 5r$	2
			Spectrum	100–180 Å, $\Delta\lambda = 0.02$ Å	4001
				Spectrum for $N_e = 5 \times 10^{18}$ only	

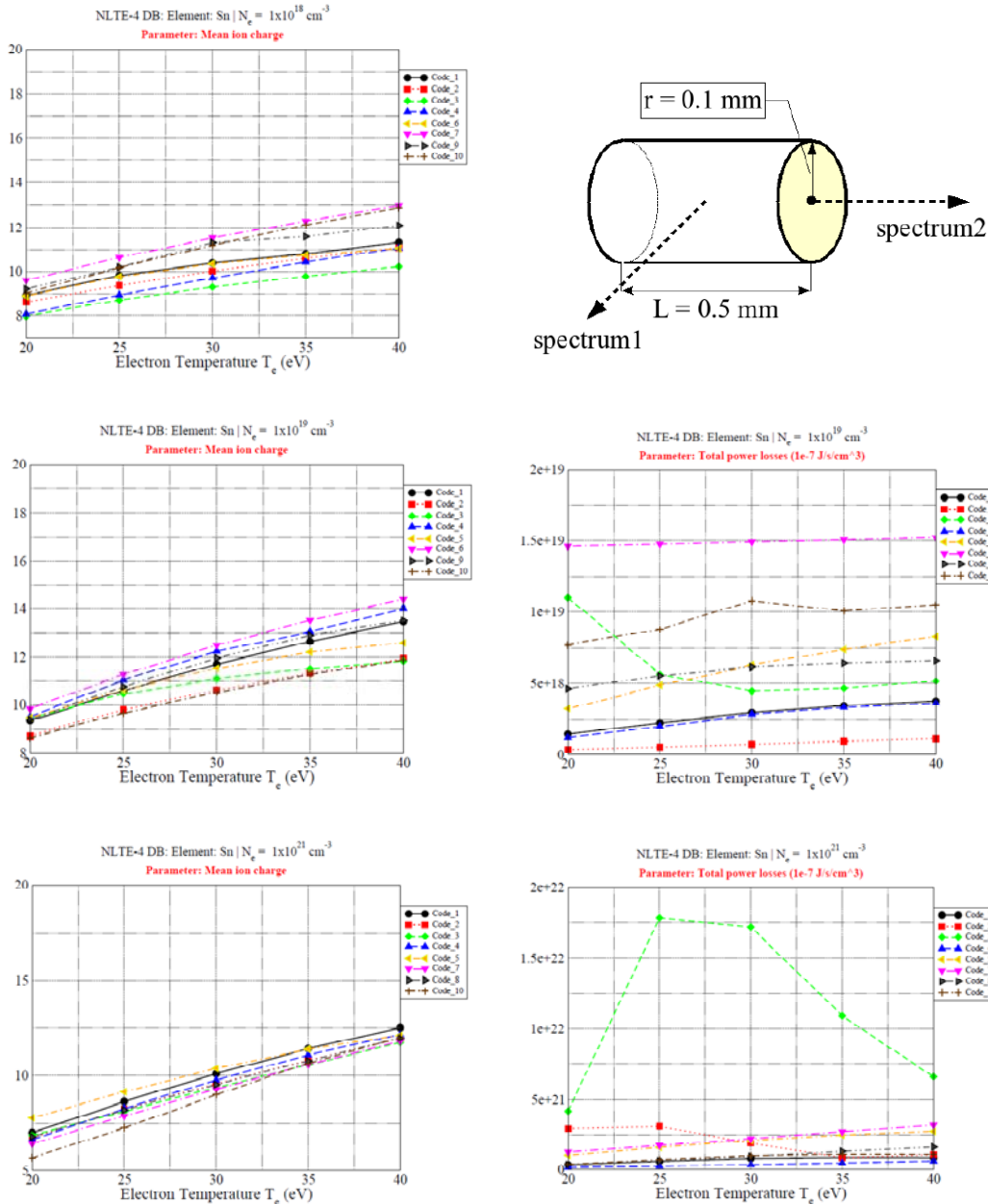


Figure 3.a. Tin plasma properties with participant codes of NLTE-4 Workshop. Thick cases by a uniform cylinder of radius 0.1 mm

Table 3.a: Tin optically thin plasma properties of ATMED CR for comparison with codes of NLTE-4 Workshop

$r = 0 \text{ mm} \&$ $N_e (\text{cm}^{-3}) = 10^{18}$	ρ (g/cm^3)	Z_{bar} ATMED	Z_{bar} NLTE-4	η_e ATMED CR	K_R (cm^2/g)	K_p (cm^2/g)	RPL ($10^{-7} \text{ J/cm}^3/\text{s}$)
$T_e = 25 \text{ eV}$	2.200E-05	9.048E+00	8.5±10.5	-1.3524E+01	4.438E+03	7.422E+04	8.211182E+15
$T_e = 30 \text{ eV}$	2.000E-05	1.015E+01	9.25±11.5	-1.3778E+01	5.562E+03	5.958E+04	1.406701E+16
$T_e = 40 \text{ eV}$	1.800E-05	1.137E+01	10.2±13	-1.4201E+01	6.183E+03	4.021E+04	3.135937E+16
$r = 0 \text{ mm} \&$ $N_e (\text{cm}^{-3}) = 10^{19}$	ρ (g/cm^3)	Z_{bar} ATMED	Z_{bar} NLTE-4	η_e ATMED CR	K_R (cm^2/g)	K_p (cm^2/g)	RPL ($10^{-7} \text{ J/cm}^3/\text{s}$)
$T_e = 20 \text{ eV}$	2.200E-04	8.990E+00	8.6±9.8	-1.0893E+01	7.889E+03	7.161E+04	3.570959E+17
$T_e = 30 \text{ eV}$	1.690E-04	1.172E+01	10.5±12.5	-1.1500E+01	7.240E+03	4.791E+04	9.072992E+17
$T_e = 40 \text{ eV}$	1.610E-04	1.318E+01	11.8±14.4	-1.1863E+01	2.974E+03	3.085E+04	2.034111E+18
$r = 0 \text{ mm} \&$ $N_e (\text{cm}^{-3}) = 5 \times 10^{19}$	ρ (g/cm^3)	Z_{bar} ATMED	Z_{bar} NLTE-4	η_e ATMED CR	K_R (cm^2/g)	K_p (cm^2/g)	RPL ($10^{-7} \text{ J/cm}^3/\text{s}$)
$T_e = 20 \text{ eV}$	1.128E-03	8.744E+00	8.6±9.8	-9.2865E+00	1.346E+04	7.371E+04	1.155404E+19
$T_e = 30 \text{ eV}$	8.320E-04	1.186E+01	10.8±12.4	-9.8943E+00	8.778E+03	4.670E+04	1.502173E+19
$T_e = 40 \text{ eV}$	7.060E-04	1.398E+01	12.2±14.6	-1.0325E+01	3.323E+03	2.689E+04	2.350469E+19
$r = 0 \text{ mm} \&$ $N_e (\text{cm}^{-3}) = 10^{21}$	ρ (g/cm^3)	Z_{bar} ATMED	Z_{bar} NLTE-4	η_e ATMED CR	K_R (cm^2/g)	K_p (cm^2/g)	RPL ($10^{-7} \text{ J/cm}^3/\text{s}$)
$T_e = 20 \text{ eV}$	3.000E-02	6.884E+00	6.4±8	-6.2443E+00	2.987E+04	9.324E+04	7.896211E+23
$T_e = 30 \text{ eV}$	2.100E-02	9.680E+00	9±10.5	-6.8686E+00	2.404E+04	6.128E+04	3.156075E+22
$T_e = 40 \text{ eV}$	1.700E-02	1.216E+01	11.75±12.5	-7.2837E+00	1.006E+04	3.448E+04	4.486346E+22

Table 3.b: Tin optically thick plasma properties of ATMED CR for comparison with codes of NLTE-4 Workshop

$r = 0.1 \text{ mm} \&$ $N_e (\text{cm}^{-3}) = 10^{18}$	ρ (g/cm^3)	Z_{bar} ATMED	Z_{bar} NLTE-4	η_e ATMED CR	K_R (cm^2/g)	K_p (cm^2/g)	RPL ($10^{-7} \text{ J/cm}^3/\text{s}$)
$T_e = 25 \text{ eV}$	2.200E-05	9.208E+00	8.5±10.5	-1.3507E+01	4.542E+03	7.257E+04	8.051135E+15
$T_e = 30 \text{ eV}$	2.000E-05	1.026E+01	9.25±11.5	-1.3767E+01	5.540E+03	5.862E+04	1.337473E+16
$T_e = 40 \text{ eV}$	1.800E-05	1.145E+01	10.2±13	-1.4195E+01	6.001E+03	3.979E+04	2.970821E+16
$r = 0.1 \text{ mm} \&$ $N_e (\text{cm}^{-3}) = 10^{19}$	ρ (g/cm^3)	Z_{bar} ATMED	Z_{bar} NLTE-4	η_e ATMED CR	K_R (cm^2/g)	K_p (cm^2/g)	RPL ($10^{-7} \text{ J/cm}^3/\text{s}$)
$T_e = 20 \text{ eV}$	2.200E-04	9.512E+00	8.6±9.8	-1.0837E+01	8.693E+03	6.667E+04	3.859802E+17
$T_e = 30 \text{ eV}$	1.690E-04	1.210E+01	10.5±12.5	-1.1468E+01	5.492E+03	4.548E+04	9.198930E+17
$T_e = 40 \text{ eV}$	1.500E-04	1.349E+01	11.8±14.4	-1.1911E+01	2.646E+03	2.945E+04	1.881815E+18
$r = 0.1 \text{ mm} \&$ $N_e (\text{cm}^{-3}) = 5 \times 10^{19}$	ρ (g/cm^3)	Z_{bar} ATMED	Z_{bar} NLTE-4	η_e ATMED CR	K_R (cm^2/g)	K_p (cm^2/g)	RPL ($10^{-7} \text{ J/cm}^3/\text{s}$)
$T_e = 20 \text{ eV}$	1.090E-03	9.045E+00	8.6±9.8	-9.2869E+00	1.400E+04	7.075E+04	1.056407E+19
$T_e = 30 \text{ eV}$	8.040E-04	1.228E+01	10.8±12.4	-9.8939E+00	6.712E+03	4.408E+04	1.384552E+19
$T_e = 40 \text{ eV}$	6.680E-04	1.476E+01	12.2±14.8	-1.0327E+01	2.569E+03	2.378E+04	2.100325E+19
$r = 0.1 \text{ mm} \&$ $N_e (\text{cm}^{-3}) = 10^{21}$	ρ (g/cm^3)	Z_{bar} ATMED	Z_{bar} NLTE-4	η_e ATMED CR	K_R (cm^2/g)	K_p (cm^2/g)	RPL ($10^{-7} \text{ J/cm}^3/\text{s}$)
$T_e = 20 \text{ eV}$	3.000E-02	6.898E+00	6.4±8	-6.2422E+00	2.986E+04	9.305E+04	2.814807E+22
$T_e = 30 \text{ eV}$	2.100E-02	9.714E+00	9±10.5	-6.8650E+00	2.388E+04	6.097E+04	1.494380E+22
$T_e = 40 \text{ eV}$	1.700E-02	1.223E+01	11.75±12.5	-7.2775E+00	9.765E+03	3.410E+04	1.104052E+22

2.4 Xenon Plasmas

The following problems have been established for the steady-state cases of xenon atoms on a grid of electron temperatures and electron densities, see Table 4 and Figure 4:

Element	Case ID	Total # of Points	Parameter	Grid	# of Points
Radiation power loss case					
Xenon	Xe	27	T_e	10, 20, 50, 100, 200, 500, 1000, 2000, 5000	9
			N_e	$10^{14}, 10^{18}, 10^{22}$	3

For typical values of densities as $1E+18$ and $1E+22 \text{ cm}^{-3}$, at high temperatures the autoionization rate would be used with an upper limit [2,21]:

$$A_{ji}^{kc} = C_{auto} \tanh \left[\frac{3\pi}{2\hbar} \left(\frac{\epsilon_j - \epsilon_i}{Z_{bar}} \right)^2 \frac{f_{ij}}{D_j^0} \frac{df_k}{d\epsilon} \Big|_{\epsilon=-\epsilon_k} \frac{g_A}{C_{auto}} \right] \quad (7)$$

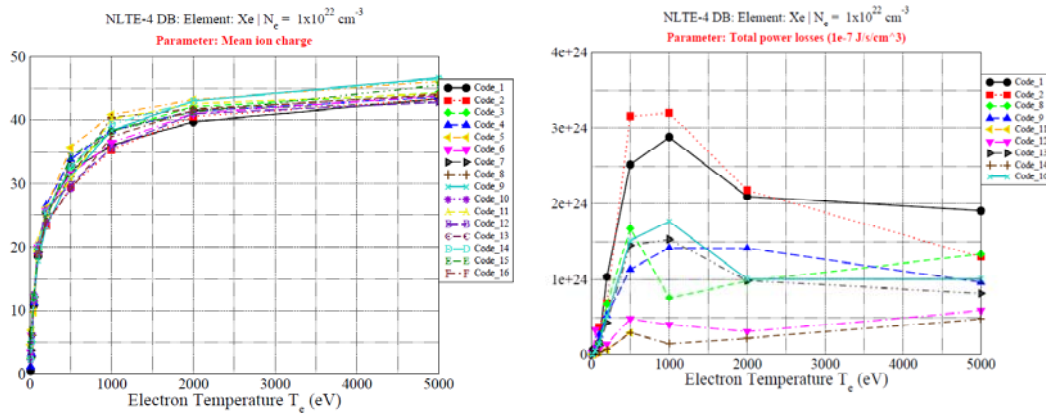


Figure 4.a. Xenon plasma properties computed with participant codes of NLTE-4 Workshop

Table 4.a: Xenon plasma properties of ATMED CR for comparison with codes of NLTE-4 Workshop

$N_e (\text{cm}^{-3}) = 10^{22}$	ρ (g/cm^3)	Z_{bar} ATMED	Z_{bar} NLTE-4	η_e ATMED CR	K_R (cm^2/g)	K_p (cm^2/g)	RPL ($10^{-7} \text{ J/cm}^3/\text{s}$)
$T_e = 20 \text{ eV}$	9.000E-01	2.548E+00	2÷7	-3.9315E+00	9.366E+04	1.333E+05	2.533781E+26
$T_e = 50 \text{ eV}$	2.300E-01	9.973E+00	9.8÷13	-5.3108E+00	1.628E+04	3.662E+04	4.102854E+25
$T_e = 100 \text{ eV}$	1.200E-01	1.850E+01	18÷21	-6.3846E+00	2.651E+03	6.972E+03	6.319852E+24
$T_e = 200 \text{ eV}$	9.000E-02	2.530E+01	23÷27	-7.3990E+00	4.610E+02	3.514E+03	3.734867E+24
$T_e = 500 \text{ eV}$	7.500E-02	2.999E+01	29÷36	-8.7859E+00	3.927E+02	1.737E+03	4.593139E+23
$T_e = 1000 \text{ eV}$	7.000E-02	3.357E+01	33÷41	-9.7820E+00	2.867E+02	7.925E+02	4.349219E+23
$T_e = 2000 \text{ eV}$	7.500E-02	3.699E+01	40÷43	-1.0656E+01	8.463E+01	3.754E+02	7.626696E+23
$T_e = 5000 \text{ eV}$	6.000E-02	3.960E+01	43÷47	-1.2185E+01	1.388E+01	7.945E+01	9.240009E+23

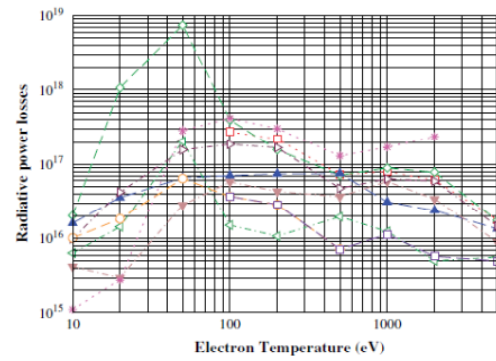
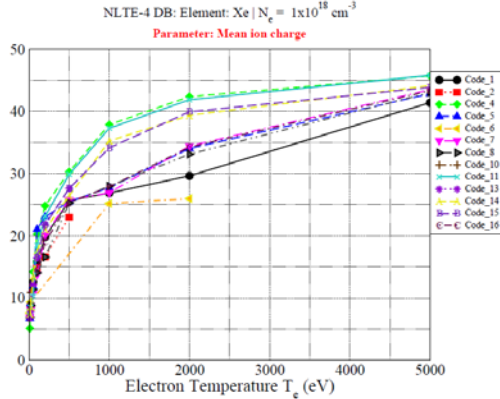


Figure 4.b. Xenon plasma properties computed with participant codes of NLTE-4 Workshop

Table 4.b: Xenon plasma properties of ATMED CR for comparison with codes of NLTE-4 Workshop

$N_e (\text{cm}^{-3}) = 10^{18}$	ρ (g/cm^3)	$Z_{\bar{\text{bar}}}$ ATMED	$Z_{\bar{\text{bar}}}$ NLTE-4	η_e ATMED CR	K_R (cm^2/g)	K_p (cm^2/g)	RPL ($10^{-7} \text{ J}/\text{cm}^3/\text{s}$)
$T_e = 10 \text{ eV}$	3.300E-05	7.142E+00	5±8	-1.2082E+01	1.048E+03	1.561E+04	1.483998E+16
$T_e = 20 \text{ eV}$	2.500E-05	8.761E+00	7.8±11	-1.3195E+01	9.298E+02	5.679E+04	5.267371E+15
$T_e = 50 \text{ eV}$	1.800E-05	1.213E+01	10±14	-1.4572E+01	4.764E+03	3.663E+04	2.678358E+16
$T_e = 100 \text{ eV}$	1.500E-05	1.550E+01	15±25	-1.5549E+01	2.062E+03	1.172E+04	1.154369E+17
$T_e = 200 \text{ eV}$	1.300E-05	1.804E+01	17±25	-1.6580E+01	1.451E+03	5.882E+03	2.733019E+17
$T_e = 500 \text{ eV}$	1.000E-05	2.349E+01	17±30	-1.7953E+01	3.870E+02	2.306E+03	4.788253E+17
$T_e = 1000 \text{ eV}$	9.000E-06	2.583E+01	25±37	-1.9003E+01	2.600E+02	1.011E+03	3.433794E+17
$T_e = 2000 \text{ eV}$	8.000E-06	2.808E+01	26±42	-2.0077E+01	9.238E+01	4.289E+02	2.503671E+17

With ATMED CR, optically coronal thin plasmas have been modeled without external radiation field and considering the Albritton's formula without upper limit for the atomic processes autoionization and dielectronic capture. The autoionization rate is calculated through the approximated expression:

$$A_{ji}^{kc} = \frac{3\pi}{2\hbar} \left(\frac{\epsilon_j - \epsilon_i}{Z_{\bar{\text{bar}}}} \right)^2 \frac{f_{ij}}{D_j^0} \frac{df_k}{d\epsilon} \Big|_{\epsilon=-\epsilon_k} g_A \quad (8)$$

Without the upper limit the splitting is of maximum importance for the bound-free oscillator strength of an electron that being bound to the nucleus, experiments a transition to the continuum. Different properties are computed if it corresponds to one or the other one between the next formulas:

- Bound-free oscillator strength formula belonging to the atomic NRSHM depending on the principal and orbital quantum numbers [2]:

$$\frac{df_k}{d\epsilon} \Big|_{\epsilon=-\epsilon_k} = f_{nl,\epsilon_c l'} = \frac{l+l'+1}{3(2l+1)} r_{nl,\epsilon l'}^2 \quad (9)$$

- Bound-free oscillator strength formula depending on the principal quantum number [8]:

$$\left. \frac{df_k}{d\epsilon} \right|_{\epsilon=-\epsilon_k} \Rightarrow \frac{f_{n,\epsilon_c}}{-\epsilon_k (eV)} = \frac{12 \frac{Q_k^4}{A} \frac{1}{n^5(k)}}{-\epsilon_k (eV)} \quad (10)$$

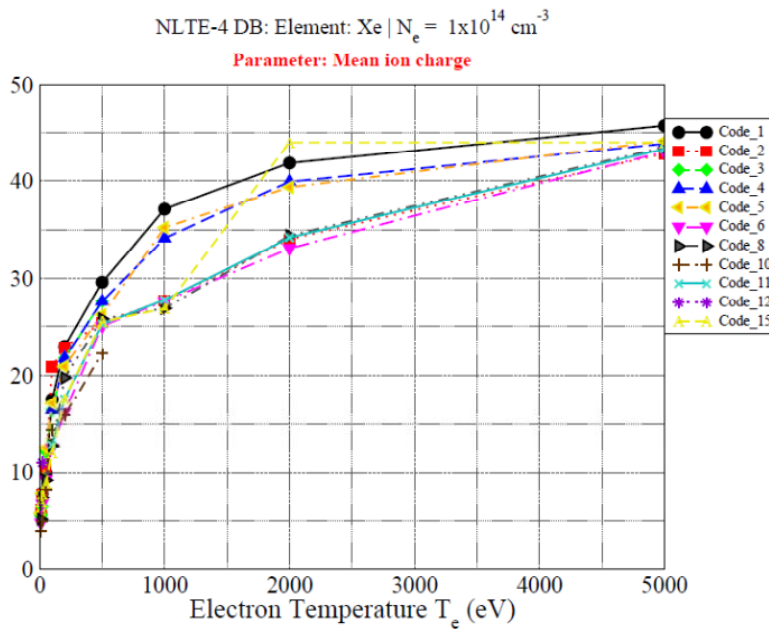


Figure 4.c. Xenon plasma properties computed with participant codes of NLTE-4 Workshop in coronal region

Table 4.c: Xenon plasma properties of ATMED CR and splitting of bound-free oscillator strength (nl) or (n)

nl-splitting & $N_e (\text{cm}^{-3}) = 10^{14}$	ρ (g/cm^3)	Z_{bar} ATMED	Z_{bar} NLTE-4	η_e ATMED CR	K_R (cm^2/g)	K_p (cm^2/g)	RPL ($10^{-7} \text{ J}/\text{cm}^3/\text{s}$)
$T_e = 10 \text{ eV}$	2.730E-09	8.035E+00	4÷10	-2.1364E+01	1.363E+01	8.131E+03	8.514073E+09
$T_e = 50 \text{ eV}$	2.150E-09	1.016E+01	10÷18	-2.3782E+01	5.165E+02	4.797E+04	1.637669E+10
$T_e = 100 \text{ eV}$	1.915E-09	1.145E+01	10÷18	-2.4818E+01	1.673E+03	1.823E+04	3.123356E+10
$T_e = 200 \text{ eV}$	1.900E-09	1.384E+01	16÷24	-2.5676E+01	2.977E+03	7.438E+03	1.420837E+11
$T_e = 500 \text{ eV}$	1.200E-09	1.818E+01	22÷30	-2.7237E+01	4.581E+02	2.784E+03	5.970642E+10
$T_e = 1000 \text{ eV}$	8.500E-10	2.571E+01	25÷37	-2.8275E+01	1.271E+02	1.017E+03	1.321816E+10
$T_e = 2000 \text{ eV}$	7.400E-10	2.952E+01	34÷44	-2.9316E+01	9.234E+01	4.237E+02	8.727946E+09
n-splitting & $N_e (\text{cm}^{-3}) = 10^{14}$	ρ (g/cm^3)	Z_{bar} ATMED	Z_{bar} NLTE-4	η_e ATMED CR	K_R (cm^2/g)	K_p (cm^2/g)	RPL ($10^{-7} \text{ J}/\text{cm}^3/\text{s}$)
$T_e = 200 \text{ eV}$	8.400E-10	2.600E+01	16÷24	-2.5862E+01	4.607E+00	3.582E+03	1.517194E+11
$T_e = 500 \text{ eV}$	8.400E-10	2.605E+01	22÷30	-2.7234E+01	2.323E+01	2.186E+03	2.739240E+11
$T_e = 1000 \text{ eV}$	8.360E-10	2.622E+01	25÷37	-2.8272E+01	1.094E+02	1.007E+03	2.453132E+11
$T_e = 2000 \text{ eV}$	5.000E-10	4.397E+01	34÷44	-2.9309E+01	2.513E+00	3.110E+02	3.228842E+12

2.5 Gold Plasmas

The following problems have been established for the steady-state cases of gold atoms on a grid of electron temperatures and electron densities:

Element	Case ID	Total # of Points	Parameter	Grid	# of Points
Comparison with experimental data; Planckian radiation field					
Gold	Au	48	T_e	400, 870, 1400, 2000, 2500, 5000	6
			N_e	$3 \times 10^{20}, 10^{21}, 3 \times 10^{21}, 10^{22}$	4
			T_{rad}	0, 175	2
			Spectrum	2.8–4.4 Å, $\Delta\lambda = 0.001 \text{ \AA}$	1601

If the upper limit used is $C_{auto} = 10^{14} \text{ s}^{-1}$ at high temperatures the values in Table 5 are obtained. This figure has been established according to Ref. [10] for matching plasma properties of a specific experiment of iron with values of temperatures at around 150 eV. Greater values more centered in the range of the rest of codes for higher temperatures can be computed with other formulas with upper limit of the order of magnitude 10^{17} s^{-1} , see References [22,23]. So this limit must be adjusted according to real experimental values for calculations.

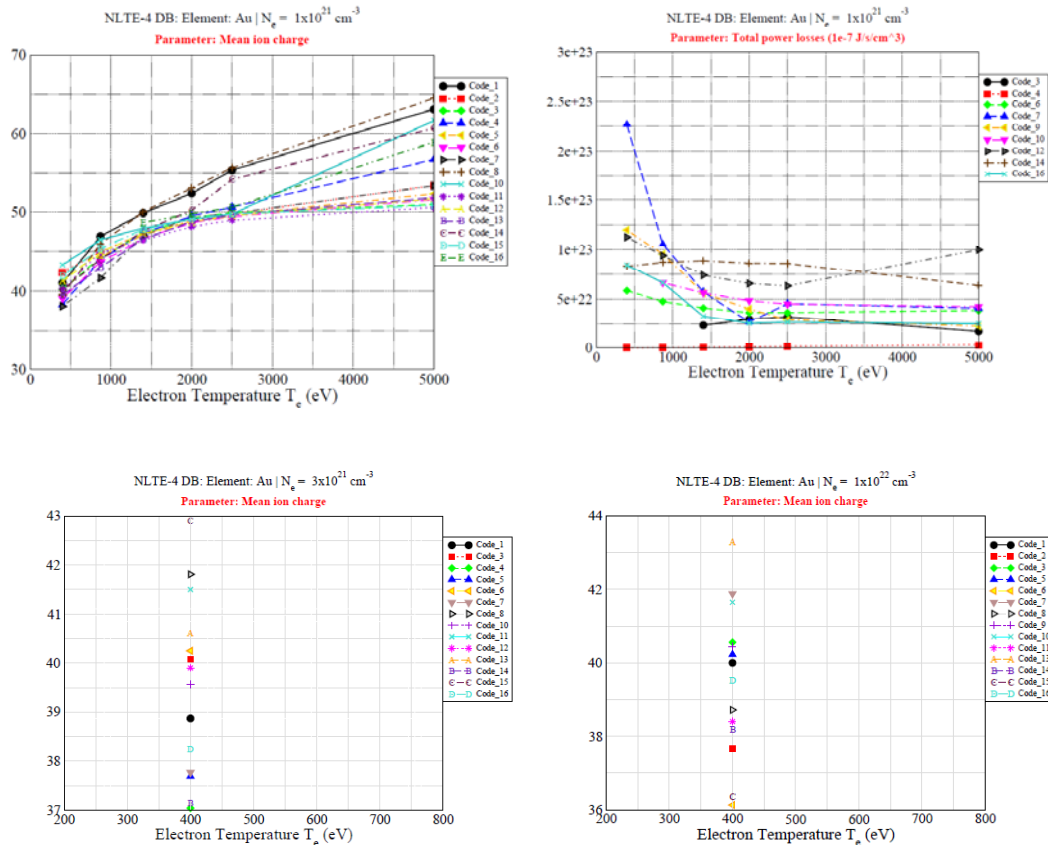


Figure 5.a. Gold plasma properties at radiation temperature $T_{rad} = 175 \text{ eV}$ computed with participant codes of NLTE-4 Workshop

Table 5.a: Gold plasma properties of ATMED CR for comparison with codes of NLTE-4 Workshop

$T_{\text{rad}} = 175 \text{ eV} \& N_e (\text{cm}^{-3}) = 3 \times 10^{20}$	ρ (g/cm ³)	Z_{bar} ATMED	Z_{bar} NLTE-4	n_e ATMED CR	RPL (1e-7 J/cm ³ /s)
$T_e = 400 \text{ eV}$	2.389E-03	4.108E+01	40÷45	-1.1989E+01	1.258219E+22
$T_e = 870 \text{ eV}$	2.298E-03	4.275E+01	42÷47	-1.3154E+01	1.359198E+22
$T_e = 1400 \text{ eV}$	2.207E-03	4.446E+01	46÷50	-1.3868E+01	1.527139E+22
$T_e = 2000 \text{ eV}$	2.136E-03	4.594E+01	49÷53	-1.4403E+01	1.106929E+22
$T_e = 2500 \text{ eV}$	2.086E-03	4.704E+01	49÷55	-1.4738E+01	4.634427E+22
$T_e = 5000 \text{ eV}$	1.991E-03	4.929E+01	49÷65	-1.5778E+01	7.409020E+21
$T_{\text{rad}} = 175 \text{ eV} \& N_e (\text{cm}^{-3}) = 10^{21}$	ρ (g/cm ³)	Z_{bar} ATMED	Z_{bar} NLTE-4	n_e ATMED CR	RPL (1e-7 J/cm ³ /s)
$T_e = 400 \text{ eV}$	8.253E-03	3.964E+01	38÷43	-1.0785E+01	1.421529E+18
$T_e = 870 \text{ eV}$	7.773E-03	4.209E+01	43÷47	-1.1950E+01	1.138915E+18
$T_e = 1400 \text{ eV}$	7.346E-03	4.453E+01	46÷50	-1.2664E+01	8.685890E+17
$T_e = 2000 \text{ eV}$	7.059E-03	4.633E+01	49÷53	-1.3199E+01	5.918562E+22
$T_e = 2500 \text{ eV}$	6.888E-03	4.749E+01	49÷55	-1.3534E+01	1.133327E+24
$T_e = 5000 \text{ eV}$	6.586E-03	4.966E+01	49÷65	-1.4574E+01	3.965581E+17
$T_{\text{rad}} = 175 \text{ eV} \& N_e (\text{cm}^{-3}) = 3 \times 10^{21}$	ρ (g/cm ³)	Z_{bar} ATMED	Z_{bar} NLTE-4	n_e ATMED CR	RPL (1e-7 J/cm ³ /s)
$T_e = 400 \text{ eV}$	2.530E-02	3.878E+01	37÷43	-9.6865E+00	4.767750E+18
$T_e = 870 \text{ eV}$	2.315E-02	4.239E+01	44÷47	-1.0852E+01	2.266840E+23
$T_e = 1400 \text{ eV}$	2.185E-02	4.492E+01	46÷50	-1.1565E+01	2.536505E+23
$T_e = 2000 \text{ eV}$	2.092E-02	4.691E+01	49÷53	-1.2100E+01	3.648669E+25
$T_e = 2500 \text{ eV}$	2.045E-02	4.798E+01	49÷55	-1.2435E+01	2.551228E+23
$T_e = 5000 \text{ eV}$	1.962E-02	5.001E+01	49÷65	-1.3475E+01	1.616903E+25
$T_{\text{rad}} = 175 \text{ eV} \& N_e (\text{cm}^{-3}) = 10^{22}$	ρ (g/cm ³)	Z_{bar} ATMED	Z_{bar} NLTE-4	n_e ATMED CR	RPL (1e-7 J/cm ³ /s)
$T_e = 400 \text{ eV}$	8.485E-02	3.856E+01	36÷43	-8.4821E+00	1.007452E+24
$T_e = 870 \text{ eV}$	7.554E-02	4.330E+01	44÷47	-9.6479E+00	4.356268E+25
$T_e = 1400 \text{ eV}$	7.170E-02	4.561E+01	47÷50	-1.0362E+01	8.475453E+25
$T_e = 2000 \text{ eV}$	6.875E-02	4.758E+01	49÷53	-1.0897E+01	3.242478E+26
$T_e = 2500 \text{ eV}$	6.740E-02	4.853E+01	49÷55	-1.1231E+01	1.006861E+27
$T_e = 5000 \text{ eV}$	6.467E-02	5.058E+01	49÷65	-1.2271E+01	3.848314E+18

The mean charge values calculated with ATMED CR are always more approximated to the ones of detailed models considering a very complete selection of configurations with respect to other selections with a more reduced number of configurations [21]. For these atomic processes ATMED CR considers all possible combinations between three energy orbitals which comply with the aforementioned restrictions on their binding energies through the formula (7). The detailed model of reference [21] has considered different types of doubly excited states, also called autoionizing states which can decay through the autoionization channel, obtaining several models denominated A, B, C and D. This way model A has the greatest number of configurations, typically, some thousands. The number of configurations in model C is around 90% of the ones included in model A, while in model D, the number is the half of that in model A.

It has been checked in the ranges of density ($1E+20 \div 1E+21 \text{ cm}^{-3}$) and temperature (1000÷1500 eV) in which there is greater discrepancy between models, see Table 5 and Figure 5, that calculations of mean charge with ATMED CR, are more similar to the results of models A and C more complete in number of selected configurations and autoionizing states [2].

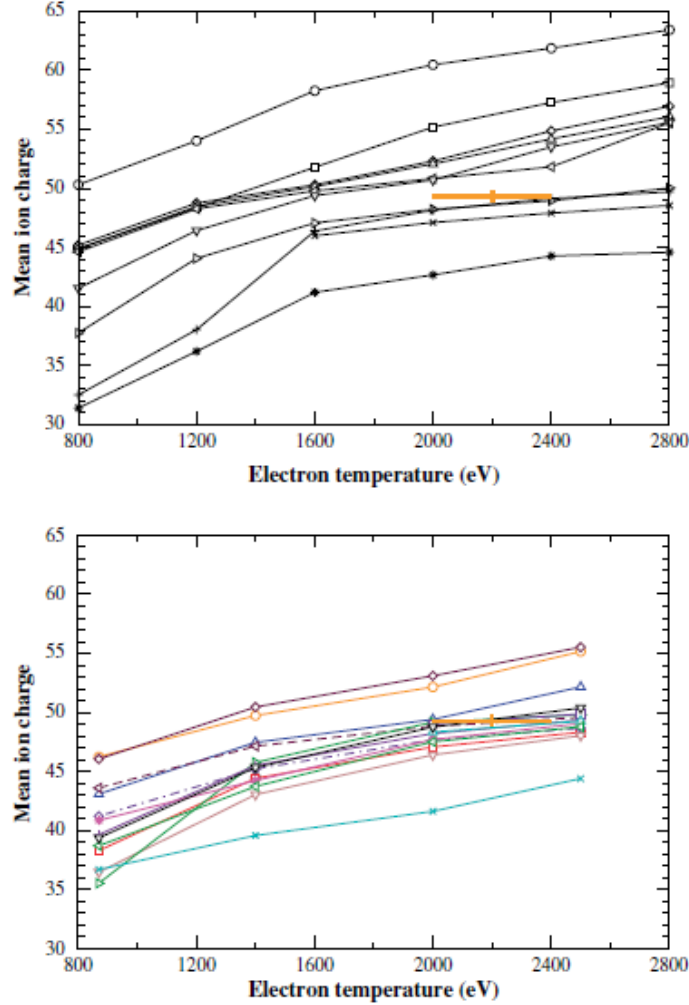


Figure 5.b. Mean ion charge for Au as a function of electronic temperature. NLTE-1 results at $N_e = 1.0E+20 \text{ cm}^{-3}$ (above); NLTE-4 results at $N_e = 3.0E+20 \text{ cm}^{-3}$ (below). The experimental value at $T_e = 2200 \text{ eV}$, $N_e = 6.0E+20 \text{ cm}^{-3}$, is $Z_{\bar{\text{bar}}} = 49.3 \pm 0.5$, in approximate agreement with the theory. Less data scatter of results obtained by codes at NLTE-4 with significant improvement in agreement in respect of NLTE-1.

Table 5.b: Gold plasma properties of ATMED CR for experimental case depending on bound-free oscillator strength splitting

BF nl-splitting & $T_{\text{rad}} = 0 \text{ eV}$	N_e (cm^{-3})	ρ (g/cm^3)	$Z_{\bar{\text{bar}}}$ ATMED	η_e	RPL ($1\text{e}-7 \text{ J/cm}^3/\text{s}$)
$T_e = 2200 \text{ eV}$	6.0E+20	4.249E-03	4.619E+01	-1.3853E+01	4.852264E+22
BF n-splitting & $T_{\text{rad}} = 0 \text{ eV}$	N_e (cm^{-3})	ρ (g/cm^3)	$Z_{\bar{\text{bar}}}$ ATMED	η_e	RPL ($1\text{e}-7 \text{ J/cm}^3/\text{s}$)
$T_e = 2200 \text{ eV}$	6.0E+20	4.200E-03	4.673E+01	-1.3853E+01	3.810040E+22

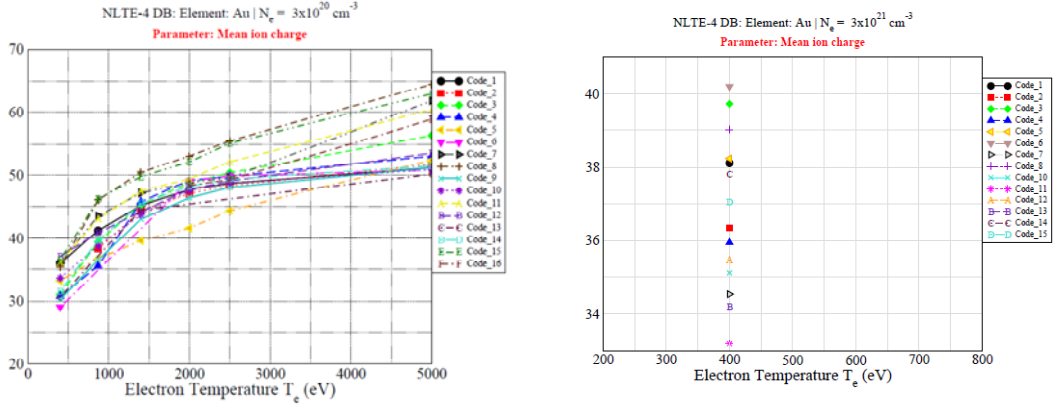


Figure 5.c. Gold plasma properties at radiation temperature $T_{\text{rad}} = 0$ eV computed with participant codes of NLTE-4 Workshop

Table 5.c: Gold plasma properties of ATMED CR for comparison with codes of NLTE-4 Workshop

$T_{\text{rad}} = 0$ eV & $N_e (\text{cm}^{-3}) = 3 \times 10^{20}$	ρ (g/cm ³)	Z_{bar} ATMED	Z_{bar} NLTE-4	η_e ATMED CR	RPL (1e-7 J/cm ³ /s)
$T_e = 400$ eV	3.427E-03	2.864E+01	28÷37	-1.1989E+01	5.986432E+18
$T_e = 870$ eV	2.850E-03	3.460E+01	35÷46	-1.3150E+01	7.725666E+21
$T_e = 1400$ eV	2.420E-03	4.079E+01	40÷50	-1.3862E+01	1.376220E+22
$T_e = 2000$ eV	2.186E-03	4.490E+01	42÷53	-1.4403E+01	1.520758E+22
$T_e = 2500$ eV	2.124E-03	4.623E+01	48÷57	-1.4737E+01	1.487068E+22
$T_e = 5000$ eV	2.025E-03	4.856E+01	50÷65	-1.5775E+01	2.801813E+22
$T_{\text{rad}} = 0$ eV & $N_e (\text{cm}^{-3}) = 10^{21}$	ρ (g/cm ³)	Z_{bar} ATMED	Z_{bar} NLTE-4	η_e ATMED CR	RPL (1e-7 J/cm ³ /s)
$T_e = 400$ eV	1.034E-02	3.167E+01	31÷38	-1.0784E+01	2.921067E+22
$T_e = 870$ eV	8.692E-03	3.764E+01	37÷46	-1.1950E+01	6.527791E+22
$T_e = 1400$ eV	7.683E-03	4.257E+01	44÷50	-1.2664E+01	7.616660E+22
$T_e = 2000$ eV	7.135E-03	4.584E+01	48÷53	-1.3199E+01	7.767916E+22
$T_e = 2500$ eV	6.940E-03	4.717E+01	49÷56	-1.3533E+01	7.783407E+22
$T_e = 5000$ eV	6.610E-03	4.948E+01	50÷65	-1.4574E+01	6.891608E+22
$T_{\text{rad}} = 0$ eV & $N_e (\text{cm}^{-3}) = 3 \times 10^{21}$	ρ (g/cm ³)	Z_{bar} ATMED	Z_{bar} NLTE-4	η_e ATMED CR	RPL (1e-7 J/cm ³ /s)
$T_e = 400$ eV	2.882E-02	3.405E+01	33÷40	-9.6863E+00	1.800489E+23
$T_e = 870$ eV	2.405E-02	4.093E+01	40÷47	-1.0849E+01	2.401587E+23
$T_e = 1400$ eV	2.212E-02	4.436E+01	47÷50	-1.1566E+01	3.490663E+23
$T_e = 2000$ eV	2.102E-02	4.669E+01	47÷53	-1.2100E+01	2.559386E+23
$T_e = 2500$ eV	2.050E-02	4.786E+01	50÷57	-1.2436E+01	2.628926E+23
$T_e = 5000$ eV	1.964E-02	4.996E+01	51÷64	-1.3475E+01	2.118830E+23
$T_{\text{rad}} = 0$ eV & $N_e (\text{cm}^{-3}) = 10^{22}$	ρ (g/cm ³)	Z_{bar} ATMED	Z_{bar} NLTE-4	η_e ATMED CR	RPL (1e-7 J/cm ³ /s)
$T_e = 400$ eV	9.013E-02	3.630E+01	34÷41	-8.4821E+00	9.711455E+23
$T_e = 870$ eV	7.686E-02	4.257E+01	42÷48	-9.6478E+00	1.341845E+24
$T_e = 1400$ eV	7.202E-02	4.541E+01	47÷50	-1.0362E+01	1.714135E+24
$T_e = 2000$ eV	6.888E-02	4.748E+01	49÷53	-1.0897E+01	1.116038E+24
$T_e = 2500$ eV	6.748E-02	4.847E+01	50÷57	-1.1231E+01	1.100801E+24
$T_e = 5000$ eV	6.469E-02	5.056E+01	52÷64	-1.2271E+01	9.142339E+23

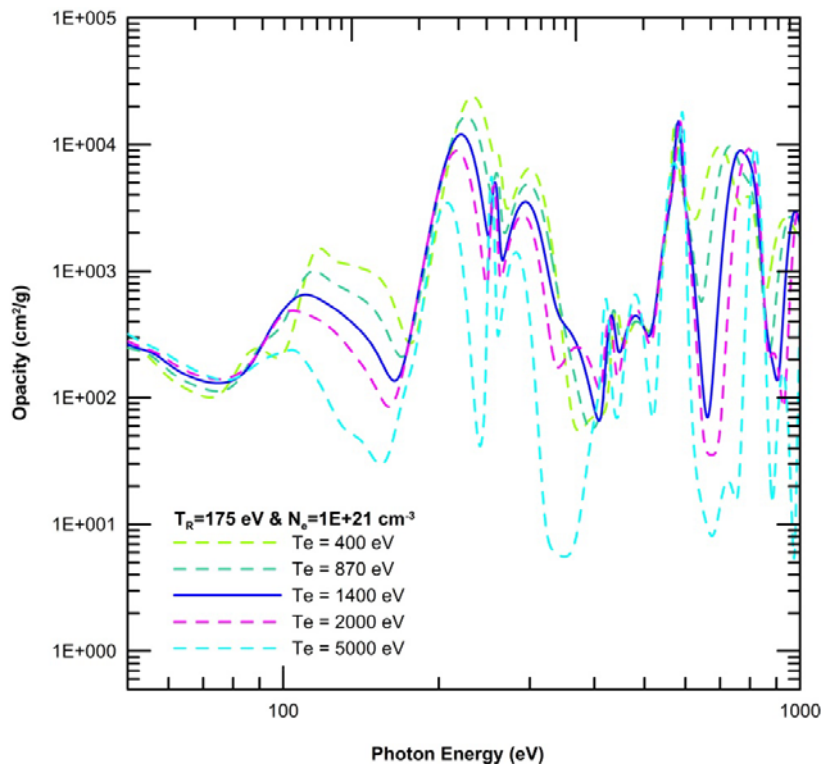
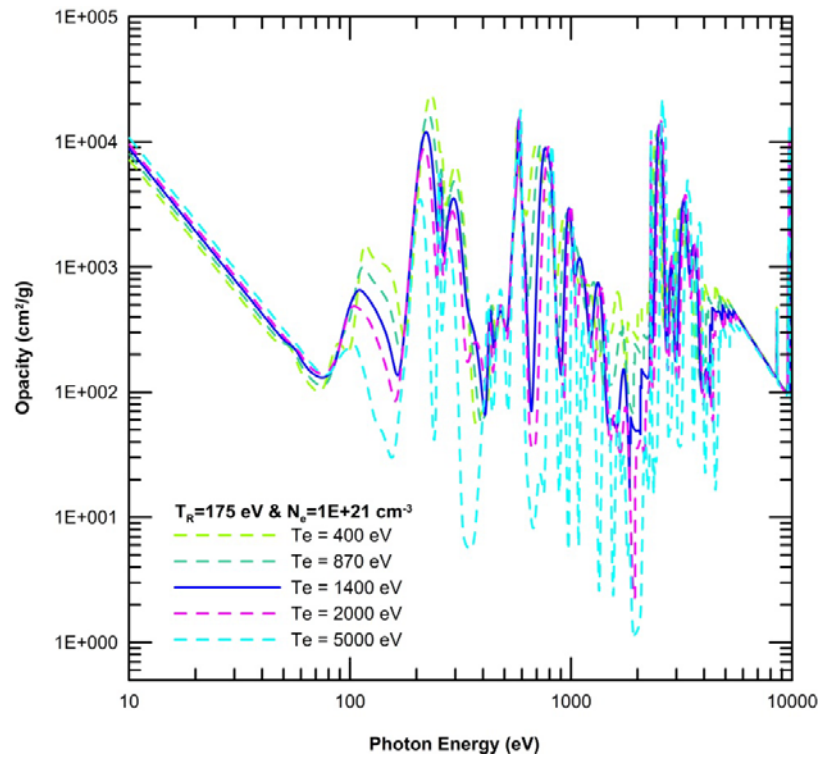


Figure 5.d. Gold plasma opacity computed with ATMED CR at radiation temperature $T_{\text{rad}} = 175$ eV at electronic temperatures in the range $T_e = 400 \div 5000$ eV and electronic density $1E+21$ cm⁻³

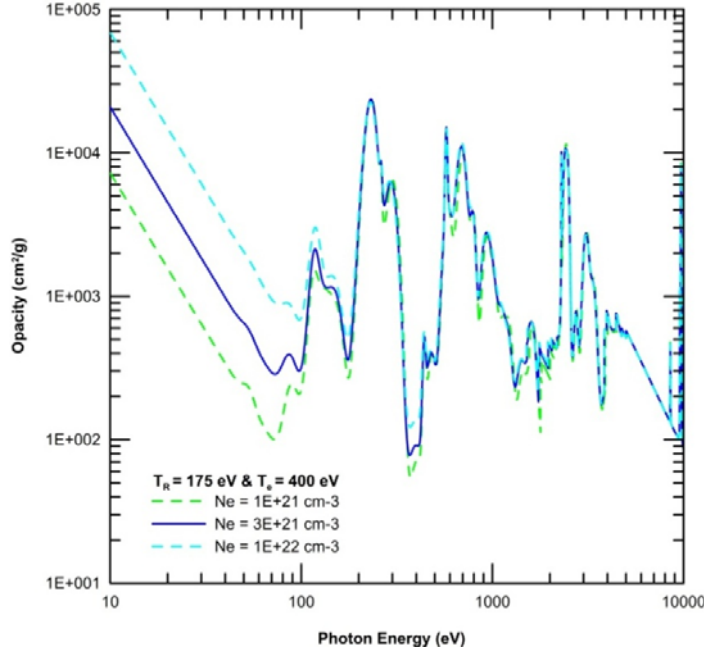


Figure 5.e. Gold plasma opacity computed with ATMED CR at radiation temperature $T_{\text{rad}} = 175$ eV at electronic temperature $T_e = 400$ eV and electronic densities in the range $1\text{E}+21\text{:}1\text{E}+22\text{ cm}^{-3}$

2.6 Radiative Properties Analysis

For high electron density, plasma self-absorption may occur. This can be observed in Figures 5.d and 5.e, where it is evident the peaked structure of opacity profile due to the great number of particles, charged ions inside the plasma acting as radiation absorbers. The following sections display a more profound analysis of radiative properties versus increasing densities for elements of a wide range of atomic numbers.

2.6.1 Dependence on Z, Density and Temperature

In Figure 6.a and Table 6 the variation of Rosseland and Planck mean opacities (cm^2/g) can be checked according to a set of parameters [14].

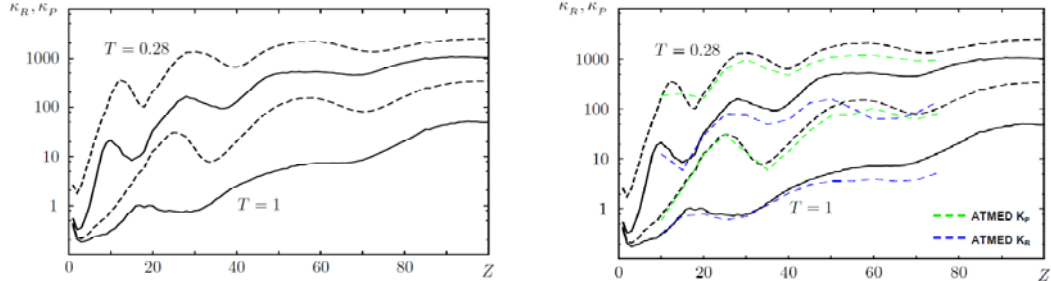


Figure 6.a. Mean opacities versus atomic number Z computed with ATMED LTE K_R (—), K_P (—) and code of Ref. [14] at conditions: electronic temperature $T_e = 1$ keV and matter density 0.1 g/cm^3 or electronic temperature $T_e = 0.28$ keV and matter density 0.05 g/cm^3

Table 6.a: Mean opacities of several elements at 280 eV and 0.05 g/cm³

ATMED LTE	Ne Z=10	Ca Z=20	Zn Z=30	Zr Z=40	Sn Z=50	Nd Z=60	Yb Z=70
K _R	1.1861E+01	2.9539E+01	7.3711E+01	6.0308E+01	1.5484E+02	6.1156E+01	7.9459E+01
K _p	1.8373E+02	1.6091E+02	9.3893E+02	4.5500E+02	1.0516E+03	1.1502E+03	8.8722E+02
CR T _e =T _R	Ne Z=10	Ca Z=20	Zn Z=30	Zr Z=40	Sn Z=50	Nd Z=60	Yb Z=70
K _R	1.518E+01	3.118E+01	8.484E+01	6.740E+01	2.261E+02	8.253E+01	8.893E+01
K _p	1.942E+02	2.081E+02	1.276E+03	6.149E+02	1.589E+03	1.797E+03	1.363E+03

Table 6.b: Mean opacities of several elements at 1000 eV and 0.1 g/cm³

ATMED LTE	Ne Z=10	Ca Z=20	Zn Z=30	Zr Z=40	Sn Z=50	Nd Z=60	Yb Z=70
K _R	3.0856E-01	7.6617E-01	6.8861E-01	2.0178E+00	3.4564E+00	3.777E+00	3.6176
K _p	5.8791E-01	1.1832E+01	1.2677E+01	1.3764E+01	7.2401E+01	9.879E+01	61.701
CR T _e =T _R	Na Z=11	Ca Z=20	Zn Z=30	Zr Z=40	Sn Z=50	Nd Z=60	Yb Z=70
K _R	3.447E-01	7.947E-01	7.251E-01	2.024E+00	3.553E+00	3.788E+00	3.854E+00
K _p	7.632E-01	1.291E+01	1.344E+01	2.030E+01	1.075E+02	1.328E+02	8.291E+01

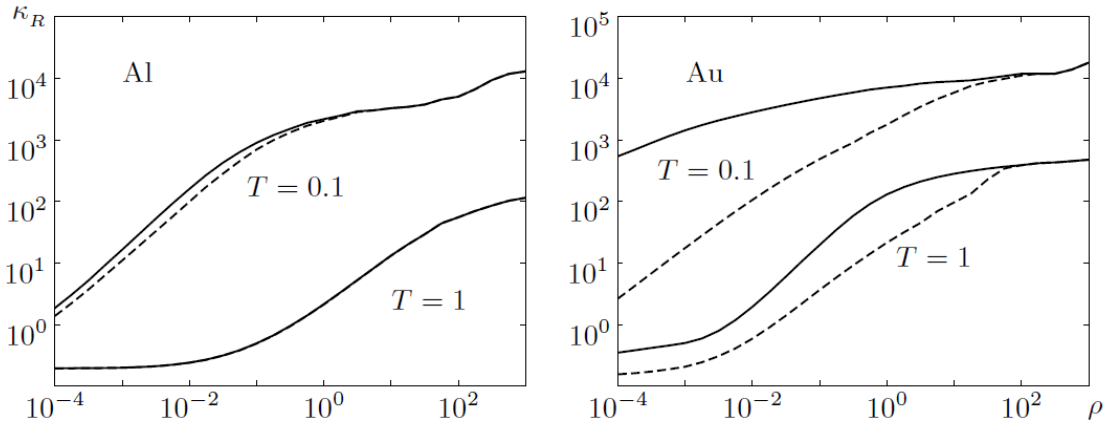


Figure 6.b. Rosseland mean opacity versus temperature in keV and density g/cm³ of aluminium and gold computed with code of Ref. [14], Figure 5.27. K_R computed considering the total opacity profiles including bound-bound transitions, this means spectral lines accounted for (solid lines) or only bound-free and free-free transitions (dashed lines). The difference between solid and dashed lines is the contribution of bound-bound transitions or spectral lines.

Table 6.c: Mean opacities of aluminium and gold plasmas with ATMED CR at conditions of Ref. [14] at high densities

Al - CR T _e =T _R	0.001 g/cm ³ – 100 eV	10 g/cm ³ – 100 eV	0.001 g/cm ³ – 1000 eV	10 g/cm ³ – 1000 eV
Z _{bar}	1.099E+01	6.435E+00	1.300E+01	1.260E+01
K _R	1.385E+01	4.212E+03	1.987E-01	1.484E+01
K _p	1.025E+02	1.917E+04	1.129E-02	1.062E+02
Au - CR T _e =T _R	0.001 g/cm ³ – 100 eV	10 g/cm ³ – 100 eV	0.001 g/cm ³ – 1000 eV	10 g/cm ³ – 1000 eV
Z _{bar}	2.956E+01	1.408E+01	6.902E+01	5.299E+01
K _R	4.592E+02	9.851E+03	4.334E-01	1.559E+02
K _p	9.187E+03	1.696E+04	2.759E+01	7.136E+02

In Figures 6.b/6.c it is clearly observed the role of bound-bound line profiles and their contribution to the total opacity profile for a light element as aluminium and a heavy one as gold. It is evident that the influence of bound-bound transition processes depends on the occupation of electrons in orbitals, being greater for elements with high atomic number Z at low densities and low temperatures.

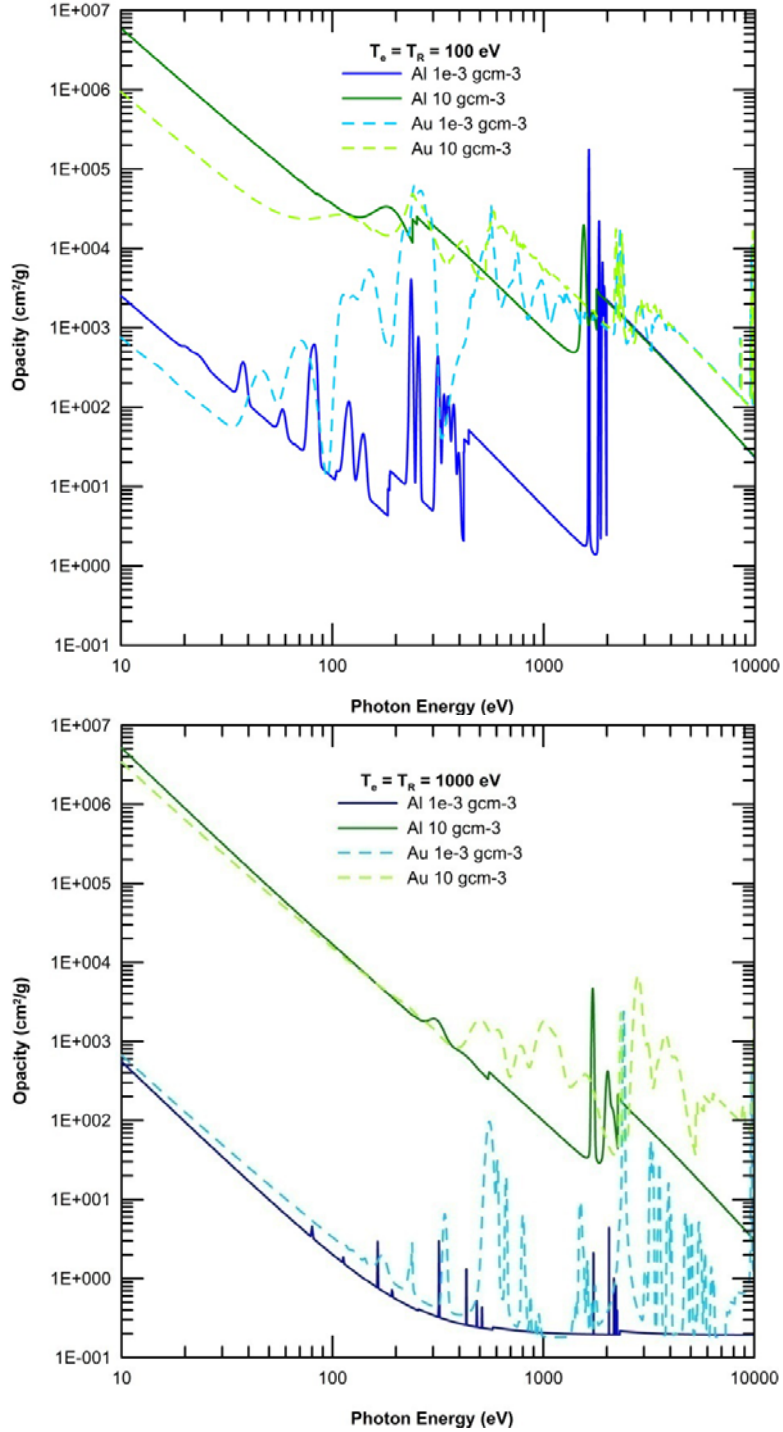


Figure 6.c. Opacity profiles of aluminium and gold computed with code ATMED CR ($T_e=T_R$) at density 10 or 10^{-3} g/cm^3 and 0.1 or 1 keV.

The spectral dependence of the absorption coefficient is determined by the importance of the different bound-bound, bound-free and free-free processes over the photon energy ranges. Besides, the influence of those processes in the Rosseland and Planck mean opacities depends on their figures at around the maximum value of their respective weighting functions in the formulas, at $3.8\div4KT$ for $\partial B_\nu / \partial T$ and $\sim 3KT$ for B_ν .

At low temperatures with the start up of ionization of each shell, the total absorption coefficient decreases but with increasing temperatures, shells become partially ionized and this coefficient rises notably due to the influence of the spectral line profiles of bound-bound processes of electronic transitions. It becomes noticeable that the photon energy range inside which the bound-bound lines have their maximum influence corresponds to conditions when the ionization makes the first shell not totally full occupied of an ion having at around the half of energy levels occupied with electrons. This way for example for gold at 1 keV and 1 g/cm³, the shell with principal quantum number $n = 3$ has at around the half of electrons of the maximum number which is possible ($Z_{\bar{b}a} = 60.88$, bound electrons according to ATMED CR and $Z_{\bar{b}a} = 60.877$ according to Ref. [14]).

2.6.2 Gold Plasmas at Low Temperatures and High Densities

In Figure 6.d it is clearly displayed for lowly ionized gold plasmas of high density the strong peak of photon absorption experimentally observed in the energy range 70÷80 eV. The figures and profiles of radiative properties computed with ATMED LTE/CR are in high concordance with experiments and also with the calculations of the collisional radiative codes of Ref. [24] in formalisms of average atom or detailed level accounting (DLA) even including the configuration interaction.

According to DLA model the biggest peak located at around 80 eV is originated from the transitions $5s \rightarrow 5p$ and $5p \rightarrow 5d$, while the structures near 100 eV are due fundamentally to $4f \rightarrow 5d$ transitions. These are the most probable transitions because of the great overlapping between orbital wavefunctions. The transitions are that of the highest contribution to Rosseland mean opacity which has a maximum value for $3.8\div4$ times the radiation temperature in the vicinity of 22.5 eV.

Table 6.d: Mean opacities of gold plasmas for comparison with figures of Ref. [24] at high densities

ATMED LTE	0.007 g/cm ³ - 22.5 eV	0.01 g/cm ³ - 23.6 eV	0.05 g/cm ³ - 27.5 eV	0.1 g/cm ³ - 29.2 eV
$Z_{\bar{b}a}$	10.17	10.23	9.946	9.744
K_R	4148.5	4770.3	8870.9	11595
K_p	31306	31462	32666	33140
CR $T_e=T_R$	0.007 g/cm ³ - 22.5 eV	0.01 g/cm ³ - 23.6 eV	0.05 g/cm ³ - 27.5 eV	0.1 g/cm ³ - 29.2 eV
$Z_{\bar{b}a}$	9.975	10.04	9.747	9.525
K_R	2.032E+03	2.350E+03	5.499E+03	8.156E+03
K_p	3.675E+04	3.617E+04	3.652E+04	3.733E+04

The higher the temperature, the peak intensity decreases for the photon absorption line profile as in Ref. [24]. With ATMED CR the intensity gradually diminishes as it is observed in Figure 6.d.

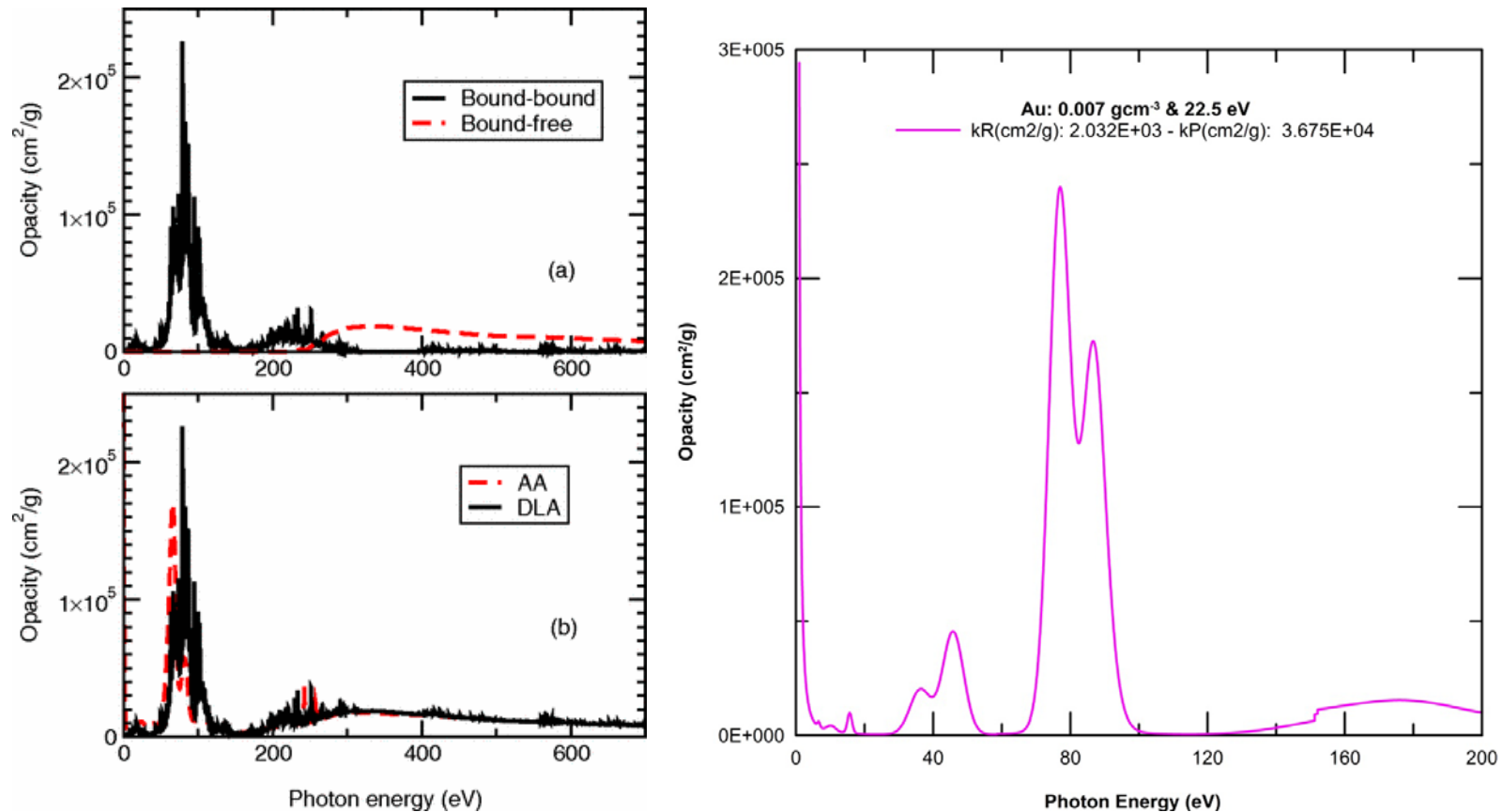


Figure 6.d1. Gold spectrally resolved radiative opacity with codes DLA (—), AA (— · —) courtesy of Ref. [24] and ATMED CR at matter density 0.007 (—) g/cm^3 and electronic temperature $T_e=T_R=22.5$ eV.

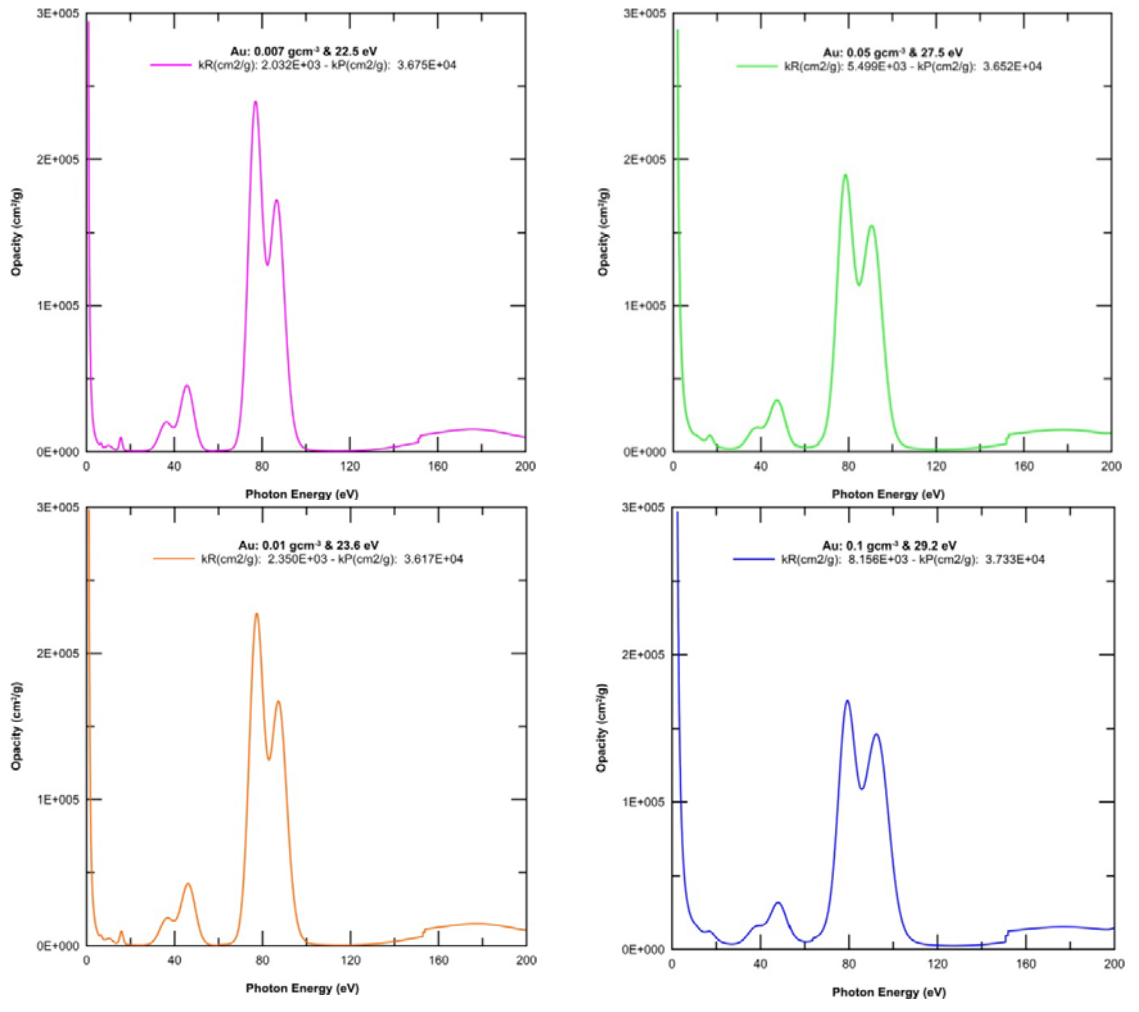
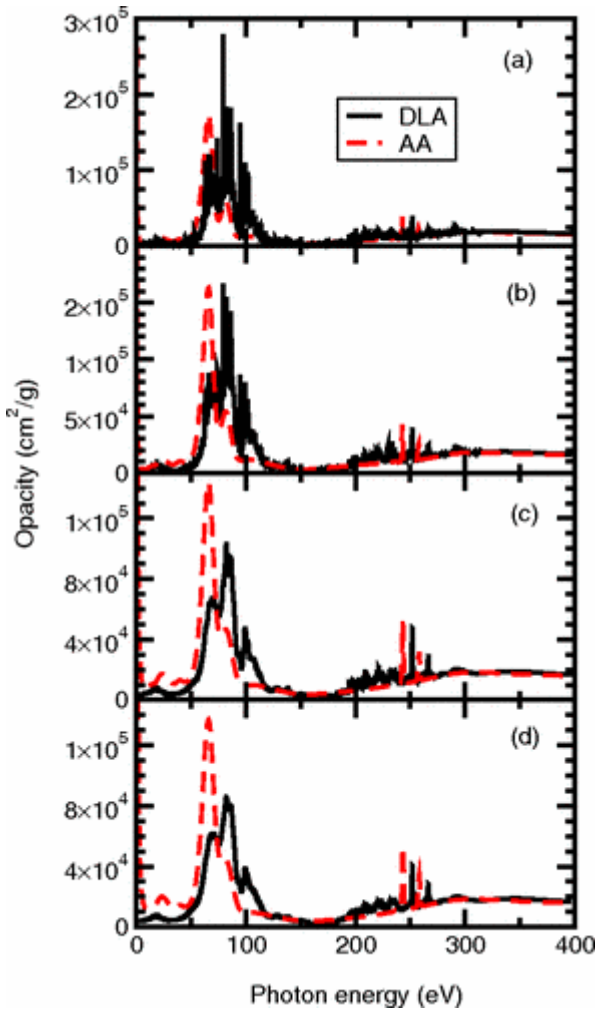


Figure 6.d2. Gold spectrally resolved radiative opacity for the $Z_{\text{bar}} \sim 10$ sequence: (a) 22 eV and 0.005 g/cm^3 , (b) 23.6 eV and 0.01 g/cm^3 , (c) 27.5 eV and 0.05 g/cm^3 and (d) 29.2 eV and 0.1 g/cm^3 computed with codes DLA (—), AA (—) courtesy of Ref. [24] and with ATMED CR at matter density 0.1 (—), 0.05 (—), 0.01 (—) and 0.007 (—) g/cm^3 and electronic temperatures respectively $T_e = T_R = 29.2, 27.5, 23.6$ and 22.5 eV.

3. SUMMARY AND CONCLUSIONS

In this paper, there are modeled with ATMED CR steady-state plasmas proposed in the 4th Non-LTE Code Comparison Workshop held in December 2005. Cases for C, Ar, Fe, Sn, Xe and Au plasmas were selected for analyzing dense plasma physics, EUV lithography sources, cold plasmas, etc., see Figure 7.

Code	Contributors	Institution	Code	C	Ar	Fe	Sn	Xe	Au	TD-Ar
ATOM3R [7]	Florido, Rubiano, Gil, Rodríguez, Minguez, <i>Mancini</i> , Martel	ULPGC/DENIM, Spain	ATOM3R	x				x		
ATOMIC [8]	Fontes, Abdallah	LANL, USA	ATOMIC	x	x	x	x	x	x	x
AVEROES [9]	Peyrusse, <i>Gilleron</i>	CELIJA/CEA, France	AVEROES	x	x			x	x	
CRETIN/CRETINL [10]	Scoi	LLNL, USA	CRETIN	x	x	x	x	x	x	x
ECRSS [11]	<i>Salzmann</i>	Soreq NRC	CRETINL	x	x	x	x	x	x	x
FAC [12]	<i>Gu</i>	Centre for Space Research, USA	ECRSS	x	x	x				
FLYCHK [13]	Chung, Lee	LLNL, USA	FAC						x	
GONDOR [14]	Bowen	CEA, France	FLYCHK	x	x	x	x	x	x	x
HULLAC v.9 [15]	Klapisch, Busquet	NRL/ARTEP, USA/France	GONDOR					x	x	
JATOM [16]	Sasaki	JAEA, Japan	HULLAC v.9	x				x		
MOST/AVE [17]	Bauche-Arnoult, Bauche	Lab. Aimé-Cotton, France	JATOM	x		x	x	x	x	
NOHEL/NOHEL2E [2]	Decoster	CEA, France	MOST/AVE					x		
NOMAD [18]	Ralchenko	NIST, USA	NOHEL					x	x	
RADIOM [19]	Bowen	CEA, France	NOHEL2E					x	x	
SCAALP [20]	Fauquier, Blanchard	CEA, France	NOMAD	x	x					x
SCRAM [21]	Hansen	LLNL, USA	RADIOM					x	x	
SCRIC [22]	de Gaufridy	CEA, France	SCAALP					x	x	
SCROLL [23]	Klapish, Bar-Shalom, Org	NRL/NRCN/ARTEP, USA/Israel	SCRAM	x	x	x	x			
THERMOS [24]	Novikov	Keldysh Institute, Russian Academy of Sciences	SCRIC	x	x				x	
XSTAR [25]	<i>Kallman</i>	NASA Goddard Space Flight Centre, USA	SCROLL		x			x	x	
			THERMOS	x	x	x	x	x	x	x
			XSTAR			x				

Figure 7. List of contributions and participant codes of NLTE-4 Workshop

The purpose of the paper is to present good results computed of ATMED CR of plasmas proposed in this scientific meeting of 2005. It has been observed a good agreement of atomic and radiative properties with respect to results of other codes which have participated in the storage inside the 4th NLTE database [18]. Iron plasmas at low electronic density 10^7 cm^{-3} can't be managed with ATMED CR.

Acknowledgements

This work has been partially supported by a Research Project of the Spanish Ministry of Science and Innovation (ENE2009-11208), by a Research Project of the “Agencia Canaria de Investigación, Innovación y Sociedad de la Información” of the regional government of the Canary Islands. (SOLSUBC2008000057) and also by the “Keep-in Touch” project of the European Union. The authors thankfully acknowledge the computer resources from Atlante, technical expertise and assistance provided by the Spanish SupercomputingNetwork (RES) and Instituto Tecnológico de Canarias Gobierno de Canarias.

References

- [1] A.J. Benita, E. Minguez, M.A. Mendoza, J.G. Rubiano, J.M. Gil, R. Rodríguez, P. Martel. Collisional Radiative Average Atom Code Based on a Relativistic Screened Hydrogenic Model. *High Energy Density Physics* 14 (2015) 18-29.
- [2] A.J. Benita. Collisional Radiative Average Atom Code With Relativistic Atomic Model. *Theoretical physics*. ISBN: 978-620-2-01943-9. LAP Lambert Academic Publishing (2017).
- [3] A.J. Benita. Fast Calculation of Plasmas Properties with ATMED LTE. Project of Nuclear Science and Technology Master at UPM (2012).
- [4] M.A. Mendoza, J.G. Rubiano, J.M. Gil, R. Rodriguez, R. Florido, A.J. Benita, P. Martel, E. Minguez. Fast Computation of Radiative Properties and EOS of Warm Dense Matter using the ATMED code. Eight International Conference on Inertial Fusion Sciences and Applications (IFSA 2013). September 8 -13 (2013) Nara, Japan.
- [5] M.A. Mendoza, J.G. Rubiano, J.M. Gil, R. Rodriguez, R. Florido, G. Espinosa, P. Martel, E. Minguez. Calculation of radiative opacity of plasma mixtures using a relativistic screened hydrogenic model. *Journal of Quantitative Spectroscopy & Radiative Transfer* 140 (2014) 81–98.
- [6] M.A. Mendoza, J.G. Rubiano, J.M. Gil, R. Rodriguez, R. Florido, P. Martel, E. Minguez. A new set of relativistic screening constants for the screened hydrogenic model. *HEDP* 7 (2011) 169–179.
- [7] F.H. Ruano, J.G. Rubiano, M.A. Mendoza, J.M. Gil, R. Rodriguez, R. Florido, P. Martel, E. Minguez. Relativistic screened hydrogenic radial integrals. *Journal of Quantitative Spectroscopy & Radiative Transfer* (2012) 117123-132.
- [8] W.A. Lokke and W.H. Grasberger. XSNQ-U A Non-LTE Emission and Absorption Coefficient Subroutine. Prepared for U.S. Energy Research & Development Administration under contract No. W-7405-Eng-48, UCRL-52276 (1977).
- [9] Joseph Abdallah et al. The reduced detailed configuration accounting (RDCA) model for NLTE plasma calculations. *High Energy Density Physics* 4 (2008) 124–130.
- [10] G.Faussurier, C. Blancard, T. Kato, R. M. More. Prigogine theorem of minimum entropy production applied to the average atom model. *High Energy Density Physics* 5 (2009) 283–293.
- [11] G.Faussurier et al. Nonlocal thermodynamic equilibrium self-consistent average-atom model for plasma physics. *PHYSICAL REVIEW E*, VOLUME 63, 026401 (2001).
- [12] Balazs F. Rozsnyai. Collisional radiative average atom model for hot plasmas. *Physical Review E* 55, (1996).
- [13] Balazs F. Rozsnyai. Hot plasma opacities in the presence or absence of local thermodynamic equilibrium. *High Energy Density Physics* 6 (2010) 345–355.
- [14] A.F. Nikiforov, V.G. Novikov, V.B. Uvarov. Quantum-statistical models of hot dense matter. *Methods for Computation Opacity and Equation of State*. Birkhäuser Verlag (2005).
- [15] A.J. Benita. Calculation of Temporal Plasmas of XFEL Experiments with a Relativistic Collisional Radiative Average Atom Code. *Physical Science International Journal*, DOI: 10.9734/PSIJ/2018/40246 (2018).
- [16] A.J. Benita. Book Summary ISBN 978-620-2-01943-9. https://www.researchgate.net/profile/Aj_Benita (2017).

- [17] A.J. Benita. Comparison of Iron Plasma Atomic and Radiative Properties Computed with a Relativistic Collisional Radiative Average Atom Code versus Other Models. *Asian Journal of Research and Reviews in Physics*, DOI: 10.9734/AJR2P/2018/41729 (2018).
- [18] <https://nlte.nist.gov/NLTE4/>
- [19] J.G. Rubiano et al. Review of the 4th NLTE Code Comparison Workshop. *High Energy Density Physics* 3 (2007) 225-232.
- [20] J.G. Rubiano et al. The 4th Non-LTE Code Comparison Workshop. Submission of Calculations. December 12-16, (2005).
- [21] Z.Q. Wu, B. Duan, J. Yan. Effects of different doubly excited states on the ionization balance and M-emissivity in high-Z plasmas. *High Energy Density Physics* 11 (2014) 70–74.
- [22] H.-K. Chung et al. FLYCHK : Generalized population kinetics and spectral model for rapid spectroscopic analysis for all elements. UCRL-JRNL-213347. *High Energy Density Physics* (2005).
- [23] H.A. Scott and S.B. Hansen. Advances in NLTE modeling for integrated simulations. *High Energy Density Physics* 6 (2010) 39–47.
- [24] Zeng Jiaolong and Jianmin Yuan. Spectrally resolved opacities and Rosseland and Planck mean opacities of lowly ionized gold plasmas. A detailed level-accounting investigation. *PHYSICAL REVIEW E* 76, 026401 (2007).